Design and Optimization of a composite rebar for the Reinforcement of concrete

Xin Yu

A thesis

in

The Department

of

Mechanical and Industrial Engineering

Presented in Partial Fulfillment of the Requirements

for the

Degree of Master of Applied Science

at

Concordia University

Montreal, Quebec, Canada

September 2003

National Library
of Canada

Bibliothèque nationale
du Canada

Acquisitions and
Bibliographic Services

Acquisisitons et
services bibliographiques

395 Wellington Street
Ottawa ON K1A 0N4
Canada

395, rue Wellington
Ottawa ON K1A 0N4
Canada

Canada

ABSTRACT

Design and Optimization of a composite rebar for the

Reinforcement of concrete

Xin Yu

In the last decade, the use of fiber reinforced plastic (FRP) composites for reinforcements to concrete members has emerged. In previous works, some design of FRP rebar that reinforced in the concrete has helical winding and some with sand coating on the outside. Different from the case of steel bar, the helical ribs here are wound on top of the bar after the bar has been pultruded. The bond between these ribs and the main bar is made of secondary bonding.

This thesis introduce a new design consists of a regular rod but it also has lobes along the rod that give the rod a wavy configuration. The reinforcement is continuous throughout the rod and the wavy part contains fibers that are part of the main rod (Rather than just bonded in). This mechanical interlock does improve the shear load transfer between the FRP rod and the concrete. The objective of this thesis is to optimize the shape of the FRP bar. Straight FRP bars and bars with circular-shaped lobes, elliptical-shaped lobes will be compared. The computer program ANSYS has been used for the finite element analysis. Optimization of the shape of the FRP bar will be discussed and the optimized shapes of the bar will be introduced.

Acknowledgements

I wish to express my gratitude and indebtedness to my supervisor, Dr. Suong V. Hoa, for continued support, guidance, and help throughout this study. I also wish to express here that Dr. Suong V. Hoa has been my constant source of inspiration for the past two years.

I am very grateful to my parents, Yu wenyuan, Huang fengling, my husband Dong xiaobo for their encouragement, support, and patience throughout the course of my study.

I also wish to thank my friends, Qi Zhao, Daying Zhang, Duosheng Xu, Lixin Wu, Weiping Liu, Yijun Jiang and Shilian Hu for their valuable suggestions, patient discussions and support during the past two years.

Table of Contents

List of Tables

List of Figures

Nomenclature

R	Radius of the bar cross section
R_c	Radius of concrete
L_b	FRP rebar length
L_c	Concrete length
X, Y, Z	Global coordinate axes
μ	Friction coefficient between the bar and concrete
N	Normal force on the bar
F	Force required to pull the bar
σ_y	Radial stress
σx	Longitudinal direction stress
N	Normal force on the aluminum bar.
A	Cross section area of the bar
As	Surface area of the bar
α	Expansion coefficient
SX	X direction stress
SY	Y direction stress
SZ	Z direction stress
SXY	XY direction shear stress
SYZ	YZ direction shear stress
SXZ	XZ direction shear stress

a	Elliptical shaped lobe major radius
b	Elliptical shaped lobe minor radius
L	Distance between two circular-shaped lobes center
L_e	Distance between two elliptical-shaped lobes center
R	Circular shaped lobe radius
E	Young's Modulus
ν	Poisson's ratio
G	Shear modulus
X_{1decay}	Distance of stress decay on left side of the lobe
X_{2decay}	Distance of stress decay on right side of the lobe
D	Distance between the two FRP rebars with circular-shaped lobes
D_e	Distance between the two FRP rebars with elliptical-shaped lobes
ε_{shu}	Time-ultimate shrinkage strain
ε_{sh6}	Time-ultimate shrinkage strain from standard 6 inches (150mm) test specimens
Ac/Pc	Cross sectional area-to-perimeter ratio
H	Ambient average relative humidity as a decimal
e_{th}	Coefficient of thermal expansion for the concrete
ΔT	Temperature drop
a_1	Inner radius of the cylinder
b_1	Outer radius of the cylinder

p_i	Uniform internal pressure
p_0	Uniform external pressure
r_1	Radius at any point of cylinder cross-section
σ_r	Radial stress
σ_θ	Hoop stress
ε_θ	Hoop strain

Chapter 1

Introduction

1.1 Background of the problem

The most commonly used construction material throughout the world is steel reinforced concrete. However, good concrete quality cannot always guarantee the protection of concrete structures against different deterioration mechanisms, such as steel corrosion [1].

The corrosion of steel reinforcement is the most common cause of failure of concrete structures. In structures such as bridges and parking garages, this fact is attributed in large part to the use of deicing salts in cold climate regions. In other parts of the world, concrete structures are continually exposed to ground and atmosphere charged with salts, accelerating the corrosion process. The cost of rehabilitation has become a major concern [2].

Poor quality concrete also contributes to corrosion. Inadequate specifications and construction practices produce concrete with high permeability and undesirable cracking which enables the ingress of corrosion-inducing agents to the reinforcing

steel, thus accelerating the corrosion process [1]. Refer to Figure 1.1. It shows that in some old bridge structures concrete is beginning to crack, some parts of the steel bars have been exposed. It is very dangerous to the whole structure and it will cost a lot to repair.

Figure 1.1   Corrosion of concrete structure

Concrete has been the most widely used construction material for decades and will continue to be for many years to come because of its very low cost, moldability, good mechanical properties, and availability throughout the world [3]. Therefore, engineers are searching for solutions to the corrosion problems in concrete structures. Several techniques such as epoxy-coated rebars, synthetic membranes, latex concrete, cathodic protection, special paints and sealants are developed. However, their

long-term efficiency is still questionable with regards to field experience.

Recently, fiber reinforced plastic (FRP) rebar has emerged as a promising material to enhance the corrosion resistance of reinforced concrete structures [4]. Refer to Figure 1.2. It shows the FRP rebars made of glass fiber and polyester resin. These bars have helical depressions and sand particle depressions. The helical windings make impression into the bar during the fabrication process. It is a very good material to be used with concrete because it has good corrosion resistance in aggressive environments. Also it is lightweight (1/5 the density of steel).
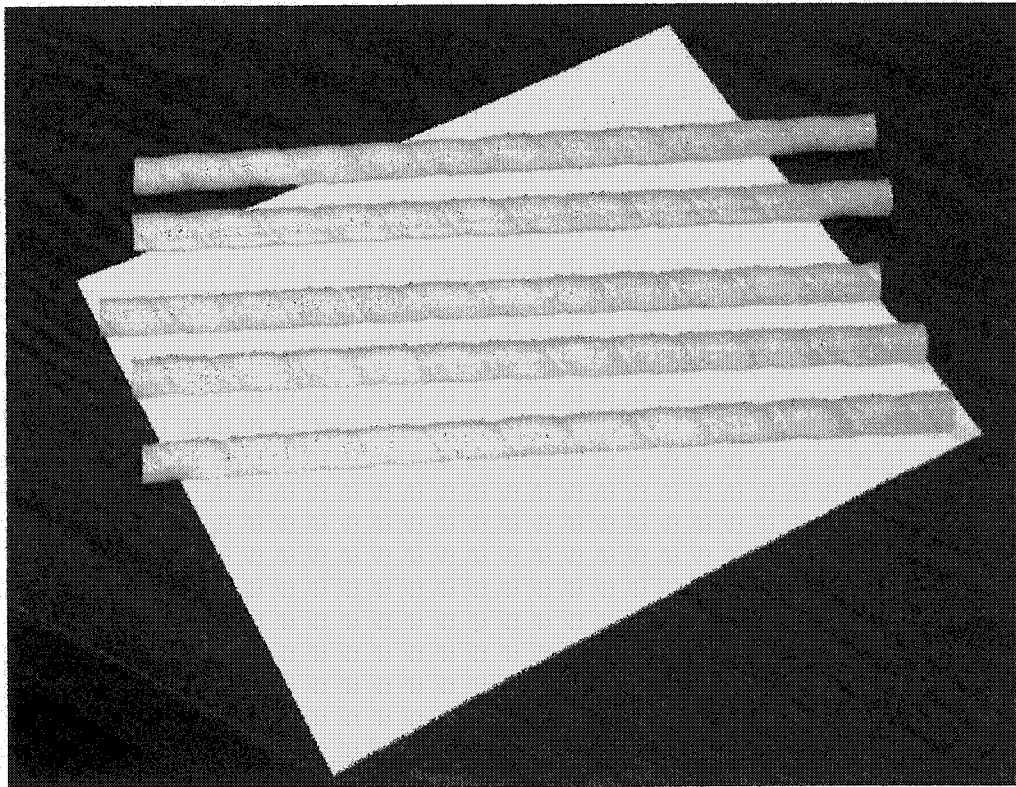
Figure 1.2   Fiber reinforced plastic (FRP) rebars

Fiber reinforced composite materials consist of fibers of high strength and modulus embedded in or bonded to a matrix with distinct interfaces between them. In this form, both fibers and matrix retain their physical and chemical identities, yet they produce a combination of properties that cannot be achieved with either of the constituents acting alone. In general, fibers are the principal load-carrying members, while the surrounding matrix keeps them in the desired location and orientation. The matrix also acts as a load transfer medium between fibers and protects them from environmental damages due to rubbing and humidity [5].

The principal fibers in commercial use are various types of glass and carbon as well as Kevlar 49. All these fibers can be incorporated into a matrix either in continuous lengths or in discontinuous (Chopped) lengths. The matrix material may be a polymer, a metal, or a ceramic [5].

Many fiber-reinforced composite materials offer a combination of strength and modulus that are either comparable to or better than many traditional metallic materials. Because of their low specific gravities, the strength / weight ratios, and modulus / weight ratios of these composite materials are markedly superior to those of metallic materials. In addition, fatigue-strength / weight ratios as well as fatigue damage tolerances of many composite laminates are excellent. For these reasons, fiber reinforced composites have emerged as a major class of structural material and are either used or being considered as substitutions for metals in many weight-critical

components in aerospace, automotive, and other industries [5].

The current fiber reinforced composite rods are made by the pultrusion process. It is a continuous molding process for producing long, straight structural members of constant cross-section area. The common pultruded products are solid rods, hollow tubes, flat sheets, and various types of beams.

Figure 1.3 is a schematic of a typical pultrusion line. Roving and mats are pulled from one end of the line into a resin bath that contains liquid resin and curing agent. Thermoplastic polyester surfacing veils are added to the fiber-resin stream just outside the resin bath to improve the surface smoothness of the product. The fiber-resin stream is pulled first through a series of preformers and then through a long preheated die. The preformers distribute the fiber bundles evenly and bring the material into its final configuration. Final shaping and curing take place in the die. Then, a number of pulling rolls or blocks pull the cured member out of the die. After cooling with air or water, it is cut into desired lengths by a diamond-impregnated saw at the end of the line [5].
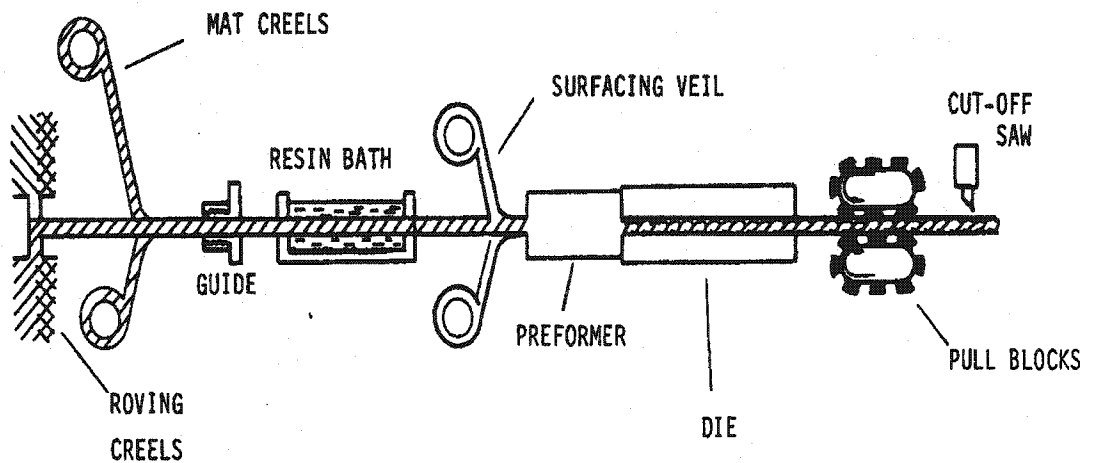
Figure 1.3   Schematic of a pultrusion process [5]

Most current fiber reinforced composite rods are usually made of glass/polyester materials. Advantages of these rods are:

● High longitudinal strength,

● Nonmagnetic,

● High fatigue endurance,

● Has potential for corrosion resistance in aggressive environments,

● Low thermal and electric conductivity,

● Lightweight (1/5 the density of steel).

Those rods also have some disadvantages

● Low ductility. Cannot be bent easily. The reason for this is because polyester is a themoset resin. Once it has cured, it does not deform easily.

- Low shear transfer efficiency. The reason for this is due to the fairly smooth surface of the rod.

- Fairly expensive. The material cost of fiber and resin are always greater than their equivalent in steel. For example, a GFRP component could cost 50% more than a steel one and a CFRP component has three times the cost of an equivalent steel component [6].

- Effect of alkali attack on glass. The corrosion attack mechanisms on glasses can vary greatly depending on the pH and strength of the attacking medium.

- Low fire resistance. When FRP reinforcement is embedded in concrete, the reinforcement can be hard to burn due to a lack of oxygen; however, the polymers will soften due to the excessive heat. The temperature at which a polymer will soften is known as the glass transition temperature. Beyond the glass transition temperature, the elastic modulus of a polymer is significantly reduced due to changes in its molecular structure [7].

1.2 Literature survey

FRP has been used in civil engineering works since the 1950s when GFRP bars were first investigated for structural use. However, it was not until the 1970s that FRP was finally considered for structural engineering applications, and its superior performance over epoxy-coated steel recognized [8]. The Japanese have the most FRP reinforcement applications with more than 100 demonstration or commercial projects. FPP design provisions were included in the design and construction recommendations of the Japan Society of Civil Engineers [7]. The use of FRP reinforcement in Europe began in Germany with the construction of a prestressed FRP highway bridge in 1986. Since the construction of this bridge, programs have been implemented to increase the research and use of FRP reinforcement in Europe. The European BRITE/EURAM Project, "Fiber Composite Elements and Techniques as Nonmetallic Reinforcement," conducted extensive testing and analysis of the FRP materials from 1991 to 1996. More recently, EUROCRETE has headed the European effort with research and demonstration projects. Canadian civil engineers are continuing to develop provisions for FRP reinforcement in the Canadian Highway Bridge Design Code [7] and have constructed a number of demonstration projects. The Headingley Bridge in Manitoba, included both CFRP and GFRP reinforcement. Additionally, the Kent County Road No. 10 Bridge used CFRP grids to reinforce the negative moment regions. The Joffre Bridge, located over the St-François River in Sherbrooke, Quebec, included CFRP grids in its deck slab and GFRP reinforcing bars in the traffic barrier and sidewalk. The bridge, which was opened to traffic in December 1997, included fiber optic

sensors that were structurally integrated into the FRP reinforcement for remotely monitoring strains [7]. More people have concentrated in the research of applying FRP materials for bridges [9][10][11]. The strength of the FRP material has also attracted engineers interest in recent years [12][13][14][15].

Many people have been concerned with some shortcomings of the current rods. For example, there are serious concerns associated with the behavior of FRP materials at high temperature, especially in case of fire [16][17]. The effect of ultraviolet rays to FRP rebar has been investigated by Tokyo University [18]. Creep and fatigue behavior, durability [19][20][21][22][23][24], moisture effect [25][26], resistance to sea water and alkali fibers of FRP rods were investigated by Tokyo Metropolitan University and other organizations [27][28][29].

Besides great amount of studies on bond behavior of FRP/Concrete systems [30][31][32] there are also a lot of investigations made to provide improved mechanical interlocking on the FRP rebars with the concrete. Benmokrane et al [33] found that smooth FRP rods, manufactured through pultrusion, suffer from weak adhesion to the surrounding concrete. Nani et al [34] indicated that additional means to improve the bond are needed. Several methods have been developed in order to improve the bond, mainly by the application of deformations on the surface using different techniques. Benmokrane et al [33] found that application of deformation by double wrapping of helical fibers around the rod significantly improved the bond.

Other means such as machined rods, embedding sand particles on the surface, and roughening by sand blasting were discussed by Cosenza et al [35]. Details of some designs are described as follows.

Groove on the bar can provide interlocking between concrete and FRP rebar. Figure 1.4 shows the FRP rebar with groove (5), which is a singular groove. In Figure 1.5, the grooves (5a) and (5b) form dual grooves that intersect with each other.
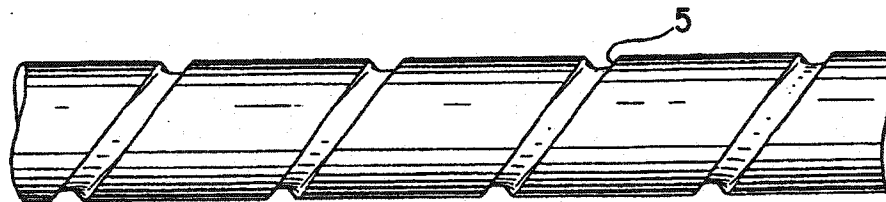
Figure 1.4   FRP rebar with a singular groove [36]
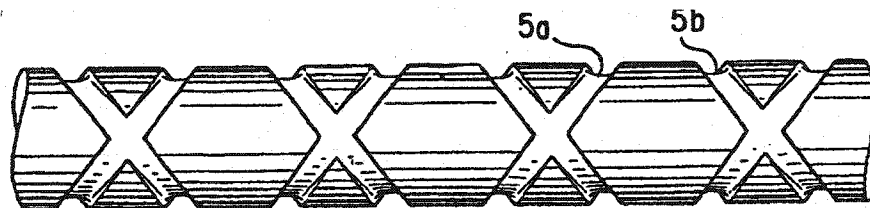
Figure 1.5   FRP rebar with grooves intersection to each other [36]

10

The rebar shown in Figure 1.6 illustrates another way to provide for mechanical interlocking. In this figure, rebar has hole (92) and flattened areas (93) that are conveniently made by crimping or crushing. In addition to providing mechanical interlocking with the concrete, the flattened areas (93) provide spots at which rebar can be more easily bent or shaped [37].
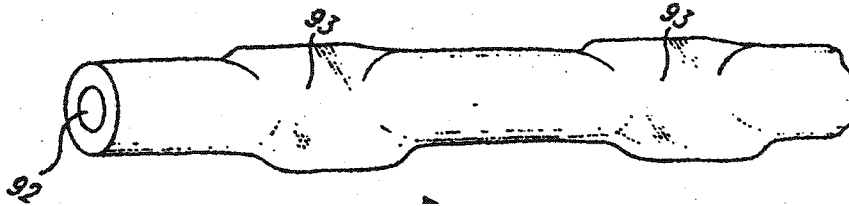
Figure 1.6   FRP rebar with flattened areas [37]

In Figure 1.7, mechanical interlocking is created by introducing curves (59) into rebar 51. Curves (59) are shown as generally sinusoidal curves, but localized curves, sharper bends and curves of other patterns are equally useful. In addition to providing sites for mechanically interlocking the rebar into the concrete, these curves tend to provide the rebar with somewhat increased elongation. When a load is applied to a curved rebar, the rebar will not break until at least some of the applied force is dissipated in straightening the bar [37].
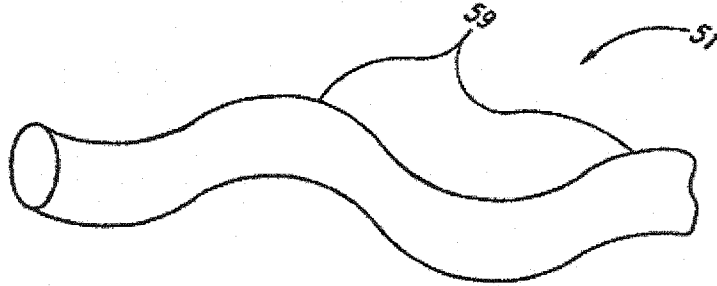
Figure 1.7   **FRP rebar with curves [37]**

Another way to provide for mechanical interlocking is to provide raised surface dimples as shown in Figure 1.8. As shown, rebar 6 has a plurality of dimples (89) that protrude from the main surface. Again, this can be done in a variety of ways. A simple way is to partially embed a suitable particulate into the surface of reinforcing rebar 6 while the thermoplastic resin is in a softened state. Suitable particulates include thermoplastic or thermoset resins, glass or other ceramic materials, metal particles, sand and other minerals [37].
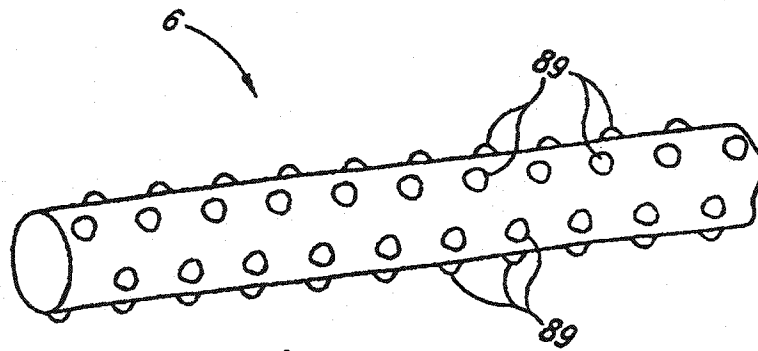
Figure 1.8   **FRP rebar with raised surface dimples [37]**

Figure 1.9 shows the FRP reinforcement disclosed in Japanese Unexamined Utility Model Publication No. 62-140115, which is formed by winding a FRP strip d on a core of a FRP rod c and bonding thereon for forming projected portions [36].
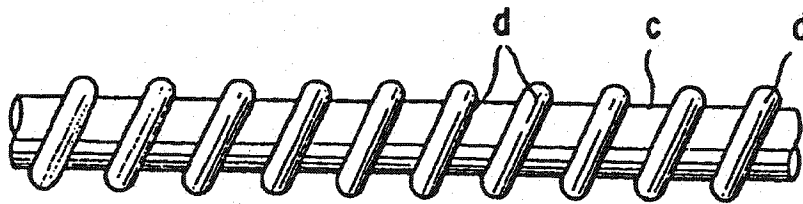
Figure 1.9   **FRP rebar with winding strips [36]**

There is another design that puts a jacket on the reinforced fibers before forming projected portions on it. Like Figure 1.10 shows, the first and second pluralities of continuous fibers can be intermixed with one another or combined as a central core of the first fibers with a jacket formed by the second fibers. The combined fibers are formed as an elongated bar or rod and rigidified using resin material [38].
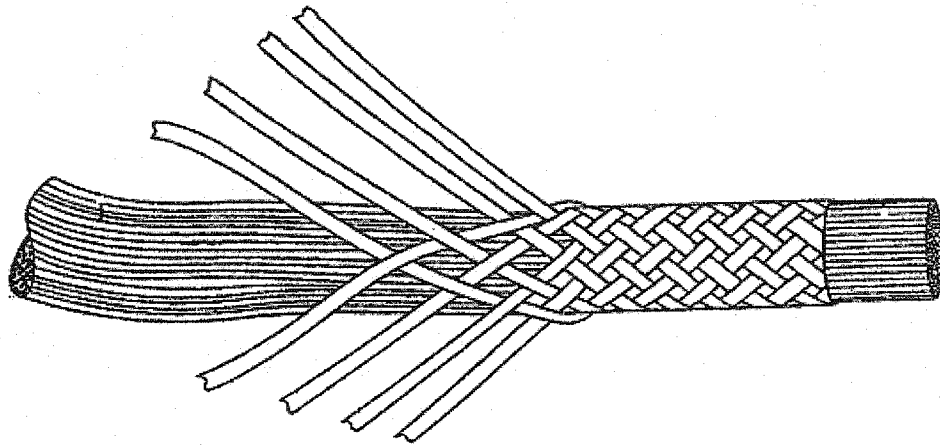
Figure 1.10   FRP rebar with a jacket formed by the second fibers [38]

Another design that provides areas of increased cross-section as shown in Figure 1.11 can create mechanical interlocking with the concrete. Areas (38) of rebar 31 in Figure 1.11 have larger cross sectional diameters than the remaining portions. This can be accomplished by over molding a thermoplastic or thermoset resin onto the rebar, especially a resin containing randomly oriented reinforcing fibers [37].

The above designs show improved interaction with concrete. However their interaction strengths with concrete are still lower than the interaction shear strengths provided by steel rods. This is probably due to the fact that the bonds between the additional roughening mechanism (Helical windings, sand particles etc.) are only bonded to the main rod by adhesive bonding, which is a weak bond [39].
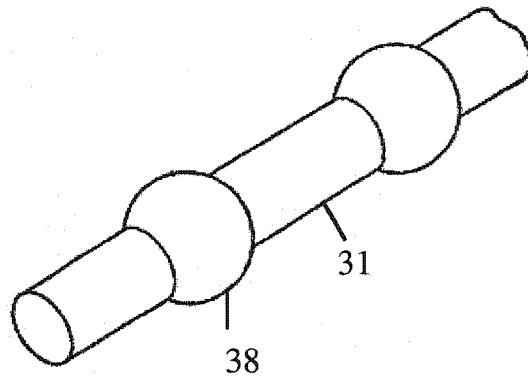
Figure 1.11   FRP rebar with lobes [37]

In the design by Hoa [39], the configuration is almost the same as that is shown in Figure 1.11. However the geometry has an integral structure of a core portion and lobe portions so that reinforcing fiber extends continuously over the core portion and the lobe portion as shown in Figure 1.12. The continuous fibers extending over the core portion and the lobe portion contribute to improve shearing strength of the lobe portion relative to the core portion in the axial direction, and as well, for improving strength against a concentrated stress at the raising edge of the lobe portion. Hoa and Xie [53] made some preliminary analysis on this new design concept. They found that the new rebar provides additional inherent mechanical interlock. The preliminary analysis also provides equations that can be used to design rebars that increase the efficiency of the reinforcement system. The bar with the new design is manufactured using a braiding process.
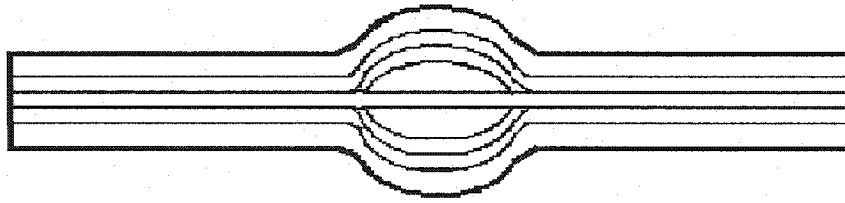
Figure 1.12   A close look at the configuration of new design
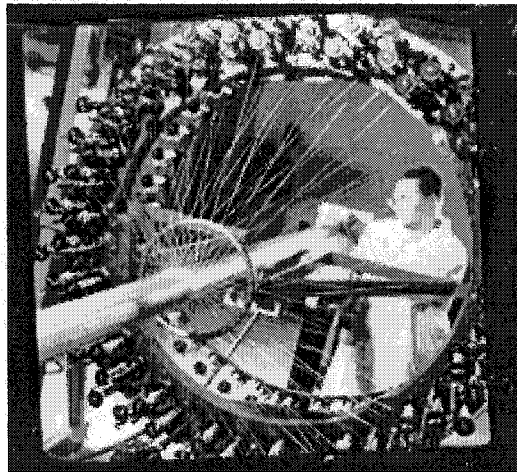
Figure 1.13   Helical braiding machine used to make the new rebar

Figure 1.13 shows the helical braiding machine used to make the new rebar. Figure

1.14 shows the details of manufacturing by braiding. The machine has creels that run

around a track plate. Fibers are fed from the creels to form the braid. The right hand

side of Figure 1.14 shows the braid configuration.

16
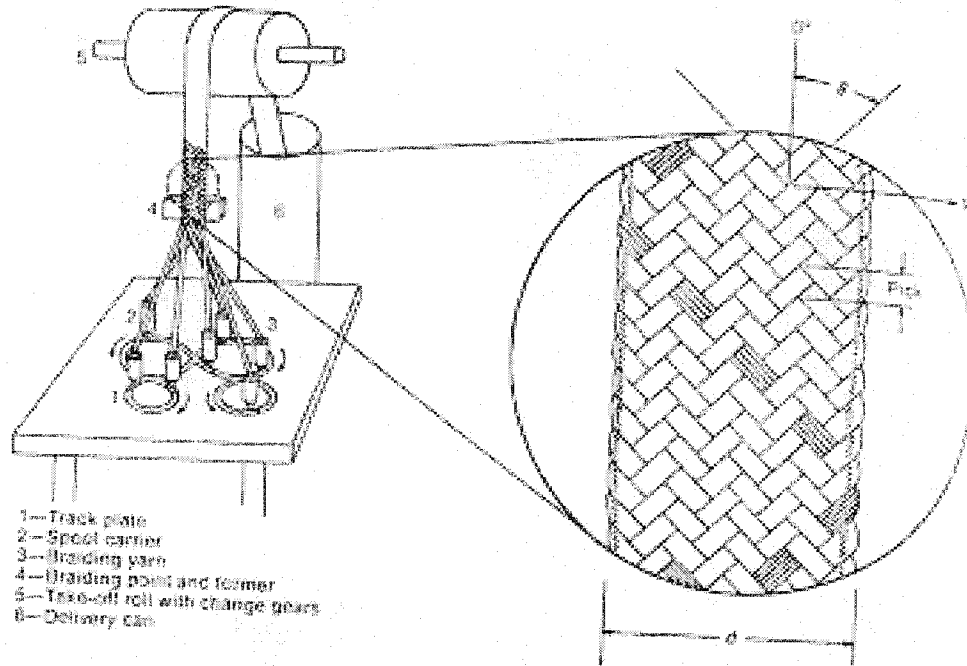
Figure 1.14   Details of manufacturing of FRP rebar

Figure 1.15a shows a sample of the new rebar. For the analysis, only one representative segment of the bar as shown in figure 1.15b is considered.
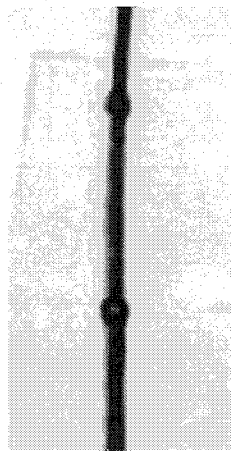
a.   **Sample of new design**
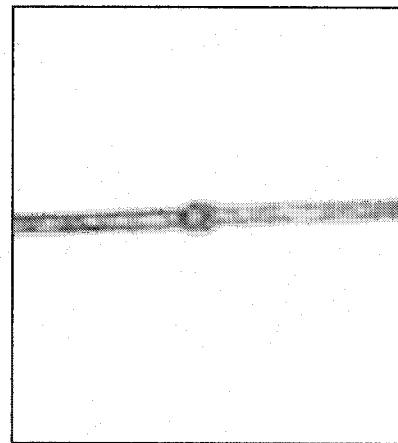
b. **One representative segment**

Figure 1.15   New design FRP rebar samples

The resin used in the new bar is thermoplastic. As such, it allows the FRP rebar to be bent easily. The following pictures show the bending test made at Concordia Center for Composites.
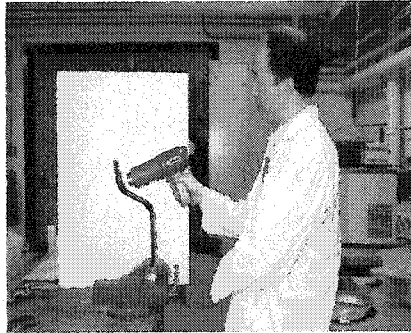
Figure 1.16   Heating the FRP rebar
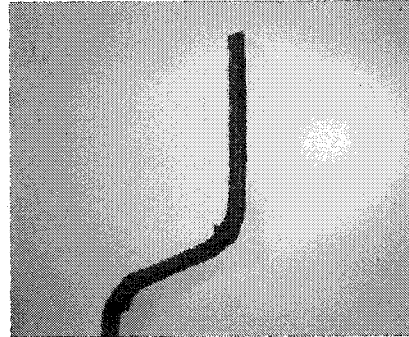
Figure 1.17   FRP rebar after bending

1.3   Objective of the thesis

The objective of the thesis is to determine the optimal design of the geometry of the new rod. Different configurations create different stress distributions in the surrounding concrete. The thesis will provide optimal shapes and configurations that can increase the efficiency of the reinforcement system.

In this thesis, Rebar with circular and elliptical lobes were studied. Software ANSYS® was used for finite element analysis.

Chapter 2

Material properties

2.1 Concrete properties

Concrete is a type of constructional material, which is used for a wide variety of purposes - as a foundation and structural material, as a wall material. It is also used for the construction of roads, airfields, buildings, water-retaining structures, docks, harbors and sea defenses. [40].

Concrete consists essentially of cement and aggregates. Cement is important constituent of concrete. There are various types of cement, like ordinary cement, rapid-hardening cement, sulphate-resisting cement, white cement, low-heat cement, masonry cement and high alumina cement. [41] Aggregates are used up to 80% by volume in ordinary concrete to provide bulk [41]. Various materials may be used as aggregate, if they are hard and do not contain anything that will decompose, or change in volume when exposed to the weather, or affect the reinforcement. The most common aggregates are sand and gravel.

Concrete is a brittle material with a compressive strength about ten times its tensile

strength. The strength of concrete increases with time and temperature. A given strength may be achieved by keeping the concrete for a long time at a low temperature or a shorter time at a higher temperature. There are also various factors that can influence the strength of concrete. The first factor is the influence of water. The strength is largely determined by the ratio of water to cement. The higher is the water/cement by weight ratio, the lower is the strength. Secondly, the strength is also affected by the total quantity of water used per unit volume. If the water/cement ratio is maintained constant but the mix proportions are varied so that less water is required per cubic yard of mix, that mix will be stronger. Thirdly, the size and shape of the aggregates, and the aggregate/cement ratio also affect concrete strength. A mix containing large aggregates up to 1.5 in. in size will have a higher strength than a mix containing smaller aggregates, and a concrete containing crushed rock will have a higher strength than a similar concrete made with rounded aggregates. Fourthly, poor mixing, poor compacting and improper curing also can result in a lower strength concrete [40].

Commonly used concretes are C15-C80 (C stands for concrete, and following digits stands for the code of the concrete). Strengths of different types of concrete are listed in Table 2.1.

Table 2.1   Young's Modulus and Strength of different types of Concrete [42]

Concrete number	C15	C20	C25	C30	C35	C40	C45	C50	C55
Young's Modulus (GPa)	22.0	25.5	28.0	30.0	31.5	32.5	33.5	34.5	35.5
Compressive Strength (MPa)	7.2	9.6	11.9	14.3	16.7	19.1	21.1	23.1	25.3

Concrete number	C60	C65	C70	C75	C80
Young's Modulus (GPa)	36.0	36.5	37.0	37.5	38.0
Compressive Strength (MPa)	27.5	29.7	31.8	33.8	35.8

Other concrete properties are shown in Table 2.2.

Table 2.2   Properties of concrete C60 [43][44][42]

Poisson's ratio	Tensile strength (MPa)	Shear strength (MPa)	Expansion coefficient α (/ °C)
0.17	3.15	3.10	12.0×10^{-6}

2.2 Shrinkage of concrete

When cement reacts with water part of the water is chemically combined, but the remainder dries out, causing the set cement to shrink. It is termed drying shrinkage [40].

The strain that occurs solely due to chemical processes in a sealed environment is termed autogenous shrinkage. Strains from autogenous shrinkage are typically small. Given the relatively small magnitude of autogenous shrinkage, it is often measured with and included in the drying shrinkage strain in the design of structures.

Drying shrinkage is not a constitutive property of concrete in that it is dependent on the size and shape of the concrete element or specimen, on the environment to which it is exposed and on the mixture parameters. The externally measured drying shrinkage strains become smaller as an element or specimen becomes more massive and/or its environment humidity increases. The internal restraint from non-linear shrinkage strain gradients in the test specimens produces stresses that reduce the axial strain component, cause cracking and stress redistribution. As relative humidity increases, shrinkage decreases and for relative humidity 98% and above, concrete swells [45]. Shrinkage is measured on specimens under the condition of zero stress; and shrinkage occurs more rapidly at the surface than at the center of the specimen [46].

For a given specimen size and exposure condition, the major factors that influence drying shrinkage include the volume of coarse aggregate, stiffness of coarse aggregate, mixing water, cement matrix volume in the concrete mixture, and the extent of the drying period. Concrete cured in high-pressure steam has very little shrinkage, while atmospheric steam curing markedly reduces shrinkage over moist curing.

When rebars are embedded in concrete during manufacturing, the shrinkage of concrete produces compressive stresses on the rebar. For the simulation of the interaction between rebar and concrete, this shrinkage needs to be studied in the model. Temperature decrease on the concrete can simulate the compression force between the concrete and the FRP rebar [47]. According to Carreira et al[47], equivalent temperature drop ΔT, is given by the following equations (1) and (2).

$$\varepsilon_{shu} = 1.2\, \varepsilon_{sh6}\, (1 - H^3)\, e^{(-0.12\, Ac/Pc)} \tag{1}$$

$$\Delta T = \varepsilon_{shu} / e_{th} \tag{2}$$

Where:

ε_{shu} Time-ultimate shrinkage strain

ε_{sh6} Time-ultimate shrinkage strain from standard 6 inches (150mm) cylinder

         shape test specimens, in micro-strains

Ac/Pc   Cross sectional area-to-perimeter ratio of specimen, in inches,

           Use (-0.00472 Ac/Pc) if units are in mm

H   Ambient average relative humidity as a decimal (e.g., H=0.7 for a relative

           humidity of 70%)

e_{th} Coefficient of thermal expansion for the concrete

ΔT Temperature drop

Different types of concrete with different conditions give different results. The

temperature range is from 27°C to 49 °C [47].

2.3 Properties of composite materials

Most composite rebars currently used are made of glass/polyester material. The reason for this is due to the relatively lower cost of glass and polyester. However, there are potential problems. One is that glass fiber is attacked by alkali solution, inherently existing in concrete. Secondly, polyester is a thermoset polymer and it cannot be bent once cured. On the other hand, carbon fibers have much better properties and are not affected by the alkali. Even though the cost of carbon fiber is relatively high at the present time, large use of the material will reduce its cost. As such, the properties of carbon composites are used in the following analysis. The material used for the manufacture of the modified rebar is made of carbon/nylon, a thermoplastic composite. Due to the lack of characterization data for this material, for simulation purposes, a composite of NCT 301 graphite/epoxy is used. This should not limit the usefulness of the results. The properties of the composite bar are shown in Table 2.3.

Table 2.3   Properties of FRP rod (Made from NCT 301

GRAPHITE/EPOXY)

Young's Modulus E_1(GPa)	113.9 [55]
Young's Modulus E_2(GPa)	7.985 [55]
Young's Modulus E_3(GPa)	7.985 [55]
Poisson's ratio ν_{12}	0.29 [55]
Poisson's ratio ν_{32}	0.4 [55]
Poisson's ratio ν_{13}	0.29 [55]
Shear modulus G_{12}(MPa)	3137 [55]
Shear modulus G_{23}(MPa)	2852 [55]
Shear modulus G_{13}(MPa)	3137 [55]
Tensile strength (MPa)	9000 [55]
Expansion coefficient α (/ °C)	24.3×10^{-6} [48]

2.4   Consideration of the effect of the reinforcement rod system on stiffness

Suitable fibers are well known such as glass fiber, ceramic fiber, carbon fiber [37].

Mixtures of different types fiber can be intermixed in order to optimize certain desired properties. For example, glass fibers can be used in the interior regions of the composite and stiffer, more expensive fibers such as carbon fibers used in the exterior regions. This permits one to obtain the benefits of the high stiffness of the carbon fibers [37].

According to Uomoto et al (1998), the FRP specimens tested are one-dimensionally reinforced FRP rods (Diameter: 6mm) of CFRP with fiber volume content of 55%. The Young's modulus is up to 1340GPa [49].

Table 2.4 shows the Young's Modulus of rod that made by NCT 301 GRAPHITE/EPOXY and some commonly used materials.

Table 2.4   Comparision of X direction Young's modulus of commonly used materials

	Steel [50]	Rod made by NCT 301 GRAPHITE/ EPOXY [55]	CFRP [7]	GFRP [7]	AFRP [7]
Young's Modulus of X direction E $_1$ (GPa)	200	113.9	120 - 580	35-51	41-125

As illustrated in Table 2.4, CFRP rebar can have a greater value of Young's modulus than steel. With the development of an appropriate manufacturing method FRP rebar could have a much higher stiffness than before.

Chapter 3

The optimization of geometry of the wavy reinforcement rod

3.1   Utilization of ANSYS® computer program

ANSYS® [51] is a computer program for finite element analysis and design. The

ANSYS® program was used to determine the optimal design for given operating

conditions.

For the concrete and FRP rebar, the elements used are SOLID92 3-D 10-Node

Tetrahedral Structural Solid. Because the lobes are circular or elliptical shapes, which

do not belong to regular shapes like rectangular or cubic this type of element is

preferred. This element is shown in Figure 3.1.
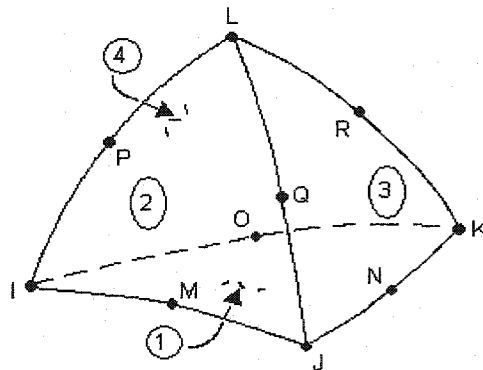
Figure 3.1   SOLID92 3-D 10-Node Tetrahedral Structural Solid element

3.2   Contact element

Since it has been observed that there is no chemical reaction between the rebar and the concrete, the situation at the interface between the concrete and the rebar is a situation of contact.

When concrete shrinks upon drying, concrete exerts a radial pressure on the rebar. This constitutes a normal force between the rebar and concrete. If an axial force is applied along the axial direction of the rod, this force has to overcome the friction force between the rebar and concrete before the rod can slide. The frictional force can be approximated as a product between the normal force and the coefficient of friction.

To simulate the interaction between rebar and concrete, the two surfaces are denoted as contact surface and target surface. The target surface usually is the harder surface and the contact surface is the softer one. If the geometry of the contact surface is different from that of the target surface, then node matching procedures have to be worked out. In the problem under consideration, the surface of the rebar was designated as the target surface and that of the oncrete was designated as the contact surface because the radial Young's modulus of FRP rebar (7.9GPa) is smaller than that of the concrete (36GPa). Since the geometry of the two surfaces is the same, the nodes on the two surfaces are the same and have the same coordinates. As such, no node matching was necessary.

For contact problems, there are two types of methods to be used. One is the Augmented Lagrange method. The other is the Penalty method. Compared to the Penalty method, the Augmented Lagrange method usually leads to better conditioning [52]. So in this study, Augmented Lagrange method was used. The concrete / FRP rebar model is a simple geometry contact model. The contact surface and target surface are smooth so that the two surfaces contact very well.

Contact 174 element (Rod) and Target 170 element (Concrete) were used for the 3D surface-to-surface contact analysis. Figure 3.2 shows the result after the contact elements were defined.
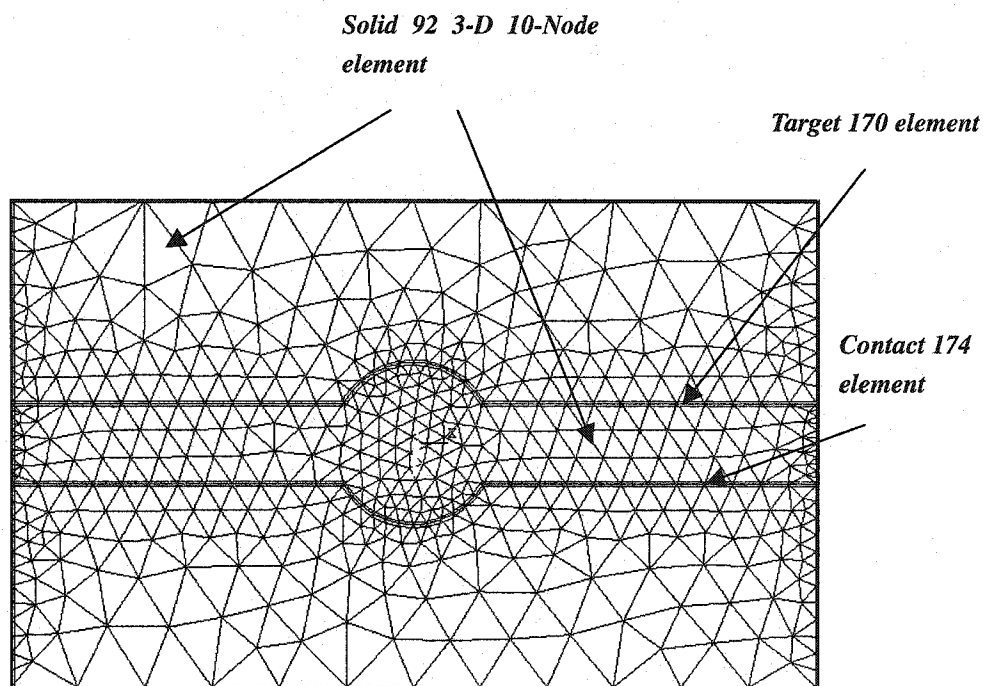
Figure 3.2   **Finite element mesh for the material system**

3.3 Modeling process

The use of ANSYS[®] for the finite element analysis in this study needs two steps, one is to build the geometry, the other is to apply the boundary conditions. According to the dimensions of the samples made at Concordia Center for Composites, the concrete cylinder used was 110mm in length and 33mm in radius; the geometry and reference frame are shown in Figure 3.3. Dimensions are shown in Table 3.1.
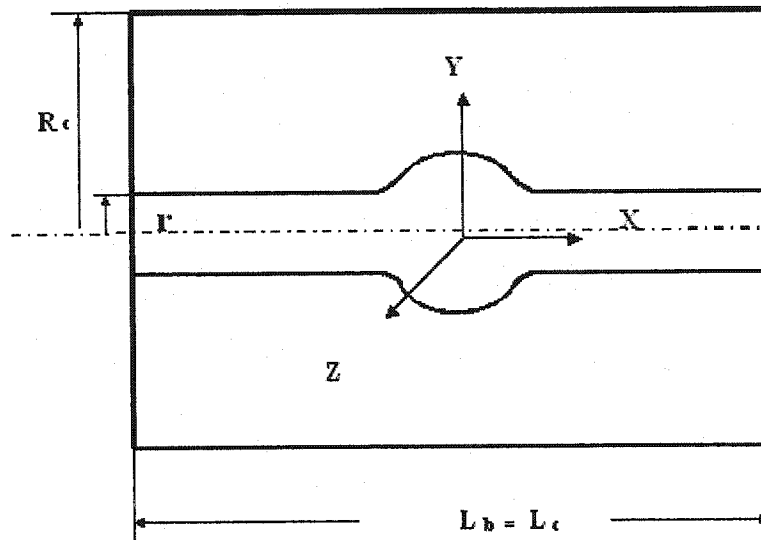
Figure 3.3   **New-design geometry and reference frame**

Table 3.1   Dimensions of concrete and FRP rebar

		Dimensions
Radius of FRP rebar	r	5.5mm
Radius of concrete	R_c	33mm
FRP rebar length	L_b	110mm
Concrete length	L_c	110mm

Due to the symmetric configuration 1/4 of the whole model was studied. Figures 3.4

and 3.5 show the configuration of the model and mesh result.
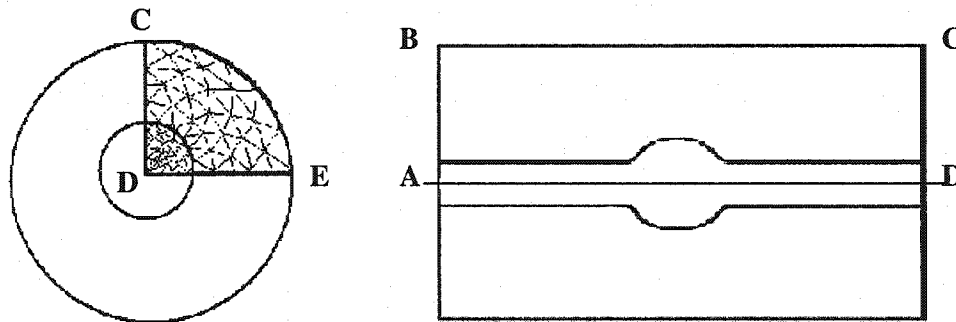
Figure 3.4   Configuration of the model
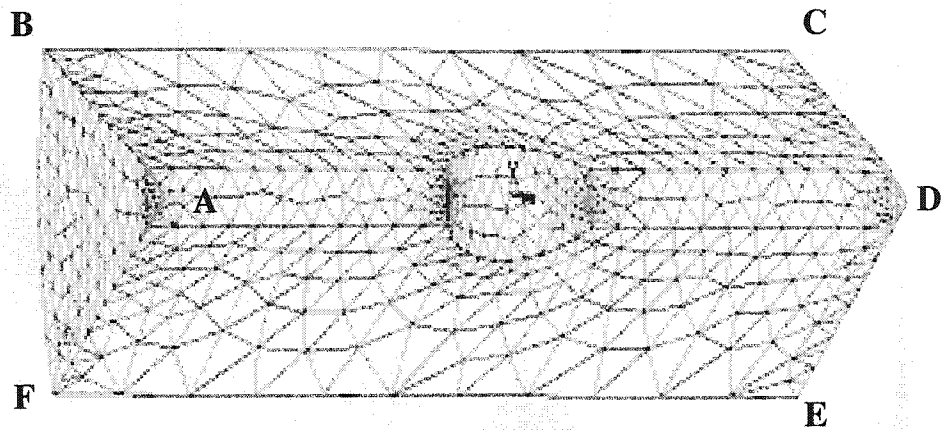
Figure 3.5   Mesh result of the model

Boundary conditions applied on the model are as follows: (As shown in Figure 3.6), the concrete was constrained on its surface (Surface BCEF) with all the degrees of freedom equal to zero. Symmetric condition applied on both two cut surfaces (Surfaces ABCD and ADEF).

Loading conditions include a pull force on the FRP rebar of 400N. That converts to a pressure is 4.2 MPa (400N / cross section area of FRP rebar).
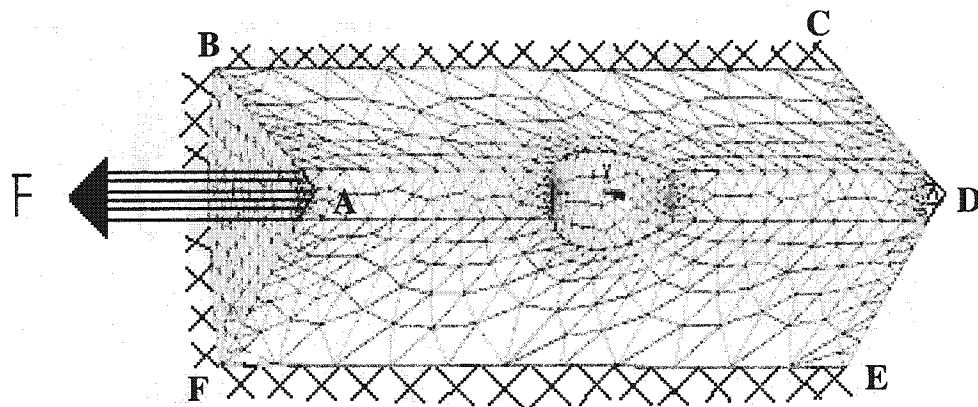
Figure 3.6   Boundary condition of the model

3.4   Verification of the modeling process

The modeling technique was verified using applied axial load only (No temperature increase on the FRP rebar). Referring to Figure 3.7, the axial stress on the rebar is given by,

$\sigma_x = F / A$

F--- Force applied on the surface

A--- cross section area of the bar

σ_x---Stress along the longitudinal direction on the FRP rebar
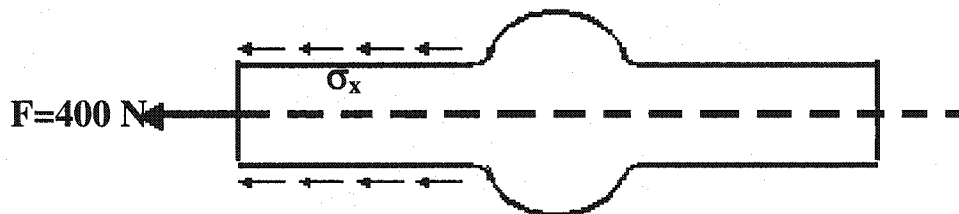
Figure 3.7   Force, Stress relationship

Substituting in the values,

$\sigma_x = F / A$

$= 400N / \pi (0.0055)^2$

$= 4.2 \text{ MPa}$

ANSYS® solution gave almost the same results. Figure 3.8 shows longitudinal

direction stress distribution on the left part of the FRP rebar.
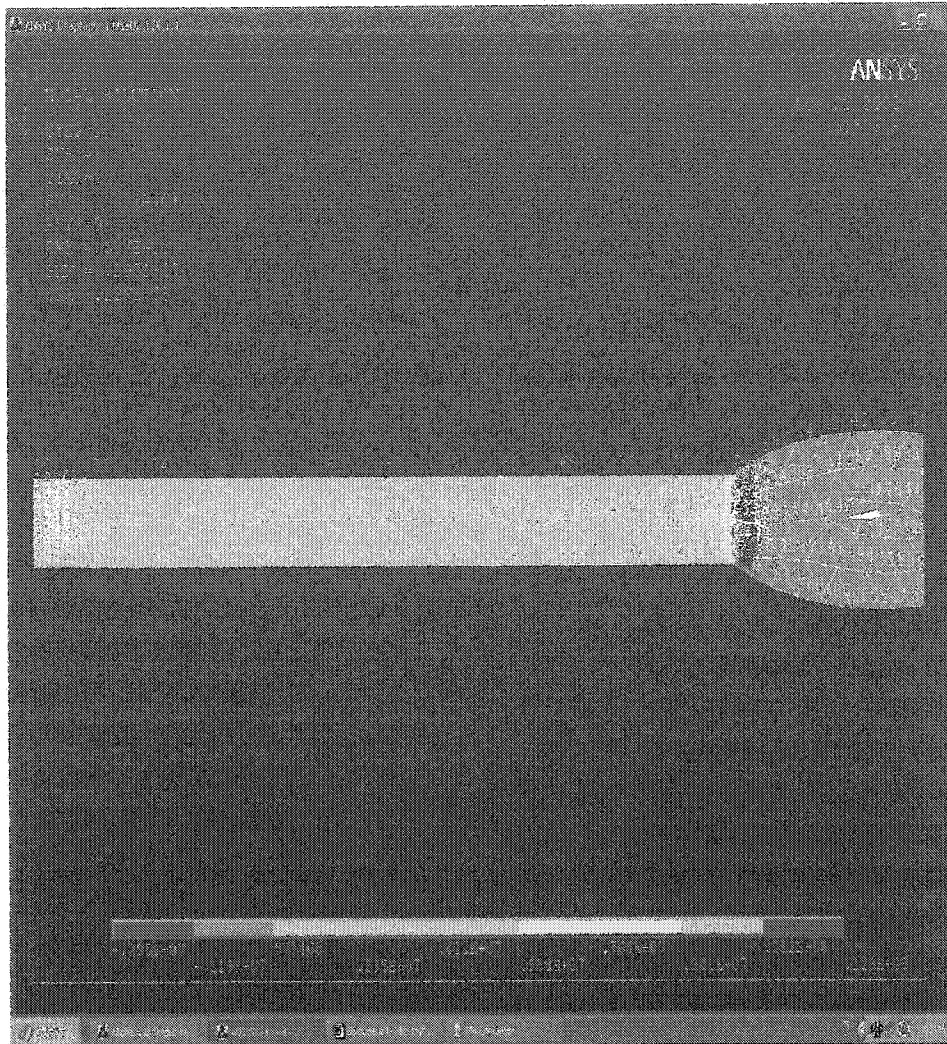
Figure 3.8   Longitudinal direction stress distribution of left part of the bar

Table 3.2 list the longitudinal stresses at the nodes along the left part of the bar.

Table 3.2   Longitudinal stresses values on the left part of straight bar

Node Number	Longitudinal Stresses (MPa)
56	4.3
58	4.3
60	4.2
62	4.1
1657	4.4
1661	4.3
1669	4.3
1668	4.3
1667	4.2
1666	4.1
628	4.4
630	4.4
632	4.3
634	4.3
636	4.2
638	4.1
Average	**4.2**

Figure 3.9 is a graph of the same result.
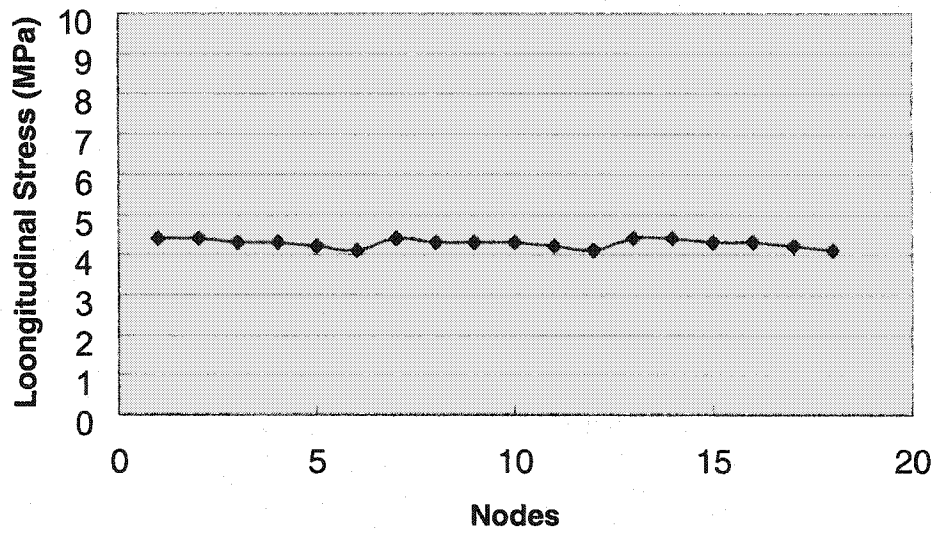
Figure 3.9   Longitudinal stress values on the left part of straight bar

From this chart, we notice the average longitudinal stress value is 4.2MPa, compared

with the value calculated by hand of 4.2MPa, and they are the same.

The above agreement provides confidence in the utilization of the program and also in

the model.

3.5   Shrinkage simulation

The drying shrinkage of the concrete needs to be considered. This shrinkage produces compressive stresses between the reinforcing rod and the concrete. This compressive stress along with the friction coefficient between rod and concrete provides the shear reaction to pull out. This needs to be considered in the model. The effect of drying shrinkage of the concrete may be simulated by contraction due to cooling of the concrete. According to reference [47], the drying shrinkage of concretes can be simulated by the thermal strains due to temperature changes in the range of 27°C to 49 °C. Temperature decrease in the concrete can create compression strains. This in turn can create a compressive force between the concrete and the rebar.

Shrinkage occurs more rapidly at the surface than at the center of the specimen. So considering the shrinkage gradient along the radial direction, a small value of temperature dropped was used. From the calculated results when the temperature drop is greater than 7 °C, models with different lobe radius fail due to concrete cracking (Tensile or shear stress exceed the strengths). Consequently, a 7 °C temperature drop was used to simulate the shrinkage in this study.

Cooling down the concrete may simulate the effect of drying shrinkage. To agree with the experimental condition that the outside surface of the concrete cylinder is constrained in the X, Y, Z directions then the simulation is not quite correct if cooling

down the concrete is used. In order to avoid this problem, rather than cooling the

concrete, the rod is heated up. If the compressive stress at the interface between the

rebar and concrete is the same in both cases (Cooling down the concrete or heating up

the rebar) then the effect is the same. Figure 3.10 shows the both cases.
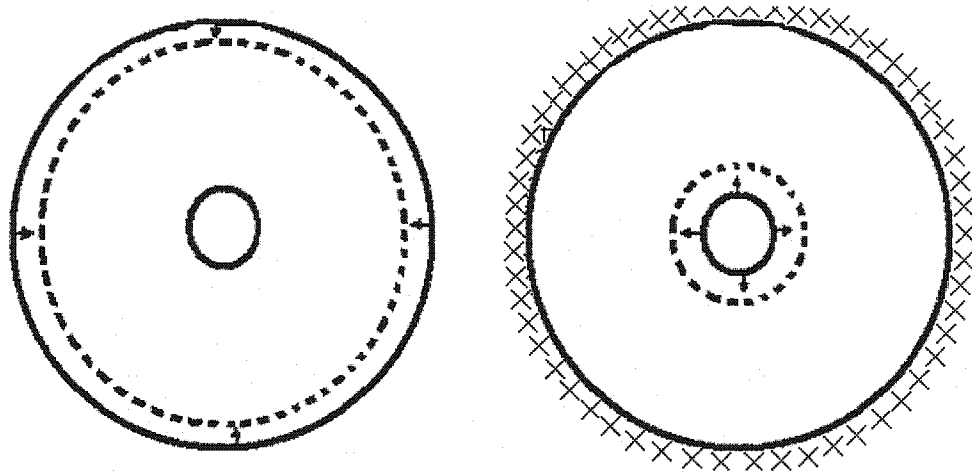
Model A. Cooling concrete only (7 °C)   **Model B.** Heating rebar only (5 °C)

Figure 3.10   Drying shrinkage in simulation

The center line of the FRP rebar was constrained. Cooling concrete only (7 °C) is

illustrated in Figure 3.10 model A. Constraining the outside surface of the concrete

and heating the rebar only (5 °C) is illustrated in Figure 3.10 model B.

Table 3.3 and Figure 3.11 show the radial compressive stress obtained from both cases.

It can be seen that cooling concrete only (7 °C) gives the same interface compression

40

stresses as the case of constraining the surface of concrete then heating rebar only (5 °C). The results are comparable within 6%, which is acceptable in this work.

Model B is also better than model A because it enables one to apply the force on the end of the FRP rebars. Model B will be selected for further work.

Table 3.3 **Radial stresses distribution on FRP rebar surface of Model A and Model B**

Nodes Number	Model A radial stresses distribution on FRP rebar surface (MPa)	Model B radial stresses distribution on FRP rebar surface (MPa)
1	−1. 15	−1. 27
2	−1. 16	−1. 25
3	−1. 16	−1. 25
4	−1. 18	−1. 25
5	−1. 08	−1. 18
6	−1. 22	−1. 37
7	−1. 23	−1. 36
8	−1. 22	−1. 31
9	−1. 23	−1. 33
10	−1. 23	−1. 37
11	−1. 23	−1. 36
12	−1. 19	−1. 37
13	−1. 13	−1. 33
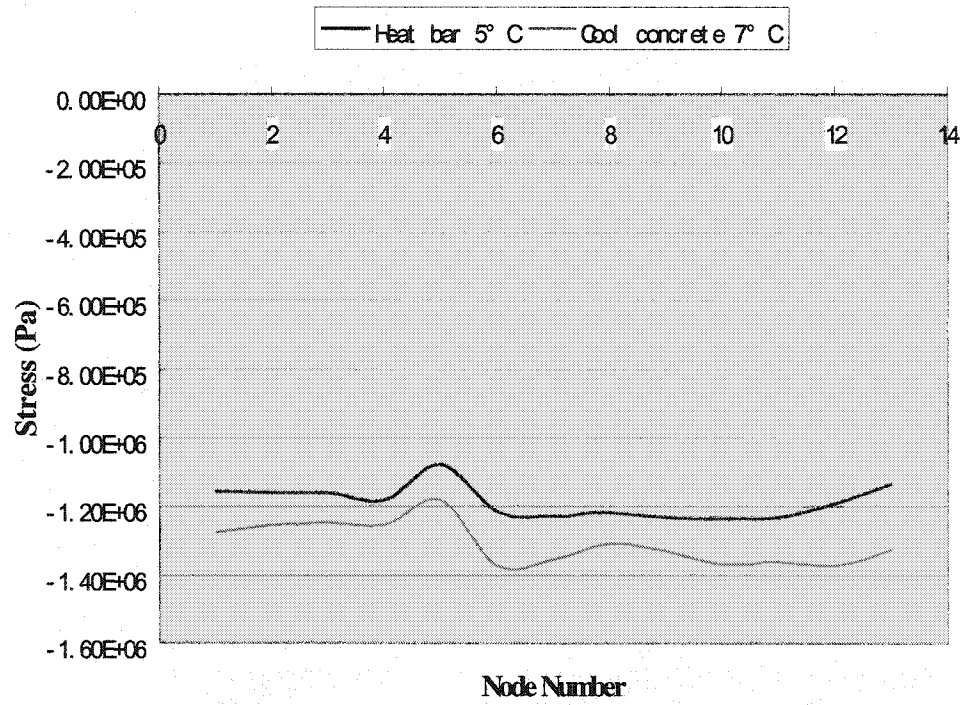
Figure 3.11   **Radial compression stress between the concrete and FRP**

rebar for the two models

3.6 Optimization parameters

As we know the controlling factor of the effectiveness of the FRP rebar is the friction and the mechanical interlock between the bar and concrete. Different lobe parameters gives different degrees of mechanical interlock. However, the existence of the lobe may give rise to higher tensile stresses in the concrete, which may cause the concrete to fail early. This may defeat the objective of improving the system. An optimal design is one that provides the maximum degree of mechanical interlock without early concrete failure. This thesis focuses on the parameter optimization. The objective is to change the lobe shape parameters to obtain maximum pull out force without tensile failure in the concrete nor slipping at the interface.
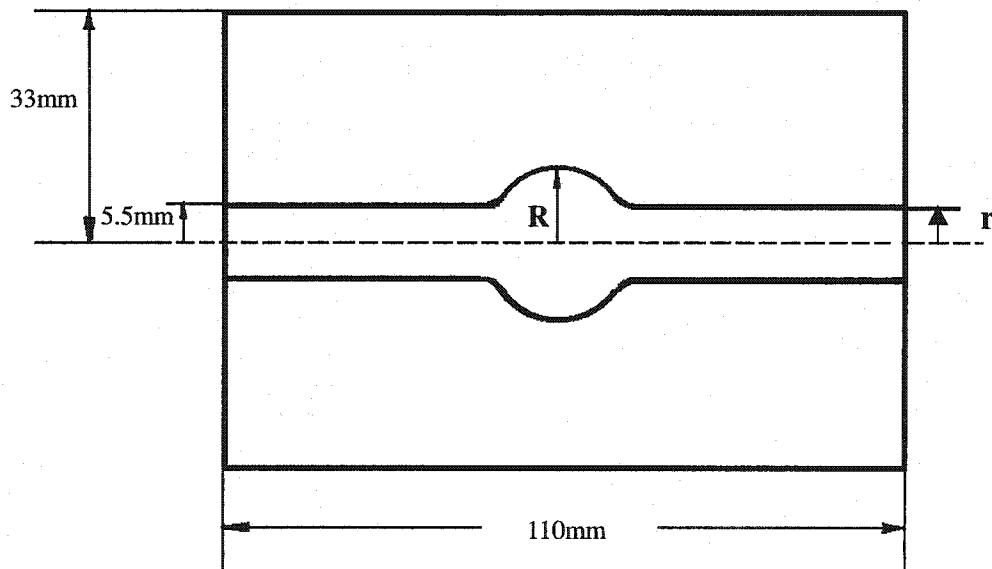
Figure 3.12   Parameters to be optimized

The optimization procedure in this study is as follows:

44

1. Fix the length of the rebar and the concrete, fix the radius of FRP rebar and concrete, and change the radius R of the lobe.

2. Determine the distance between two circular-shaped lobes on the FRP rebar.

3. Determine the distance between two FRP rebars with circular-shaped lobes in the concrete.

4. Fix the length of the rebar and the concrete, fix the diameter of FRP rebar and concrete, change the aspect ratio a/b for the elliptical-shaped lobe.

5. Determine the distance between two elliptical-shaped lobes on the FRP rebar.

6. Determine the distance between two FRP rebars with elliptical-shaped lobes in the concrete.

3.7   Criteria for optimization

Concrete fails more easily in tension due to its low tensile strength. Comparing the shear strength of concrete and FRP rebar, concrete also shows lower values, as seen in Table 3.4.

Table 3.4   Strength of FRP rebar and concrete

	Direction	FRP rebar	Concrete
Tensile strength (MPa)	SX	972.6 [55]	3.15
	SY	28.98 [55]	3.15
	SZ	28.98 [55]	3.15
Compressive strength (MPa)	SX	--	27.50
	SY	--	27.50
	SZ	--	27.50
Shear strength (MPa)	SXY	19.98 [55]	3.10
	SYZ	12.3 [55]	3.10
	SXZ	12.3 [55]	3.10

X, Y, Z direction normal strengths and XY, YZ, XZ direction shear strengths of concrete will be used to determine failure. X, Y, Z direction normal stresses and XY, YZ, XZ direction shear stresses of concrete can be obtained from calculation using the

ANSYS® program. Under the same boundary conditions and load conditions, different shaped lobes give different ratios of stress/strength, If the ratio of stress/strength > 1, failure has occured. If stress/strength < 1, the case giving the smallest ratio is the best case.

Chapter 4

Determination of optimal parameters

4.1 Rebar of fixed length, fixed diameter and circular-shaped lobe.

Determination of optimal diameter of lobe (Case 1)

Five models will be considered to evaluate the stresses on the FRP rebar as well as on the concrete. The five circular-shaped lobes models have radius of 9mm, 10mm, 11mm, 12mm, and 13mm respectively.

Other dimensions of the model except the radius of circular-shaped lobes such as length of the concrete and FRP rebar, radius of the concrete and FRP rebar are the same as shown in Table 3.1 of Chapter 3.

As mentioned in Chapter 3 Figure 3.6, boundary conditions applied were: concrete was constrained on its outside surface BCEF with all the degrees of freedom equal to zero. Symmetric condition applied on both surfaces of the cut surfaces (Surfaces ABCD and ADEF). 1/4 of the model was studied due to symmetry. The force applied on the end of the FRP rebar was 600N. Using 600N and dividing by the cross sectional area (95mm^2) of the FRP rebar, gives a pressure is 6.32MPa. The interaction

48

between concrete and FRP rebar will be simulated by heating the FRP rebar 5°C. Concrete and FRP rebar were defined in contact relation. Figure 4.1 shows the boundary conditions and loading conditions.
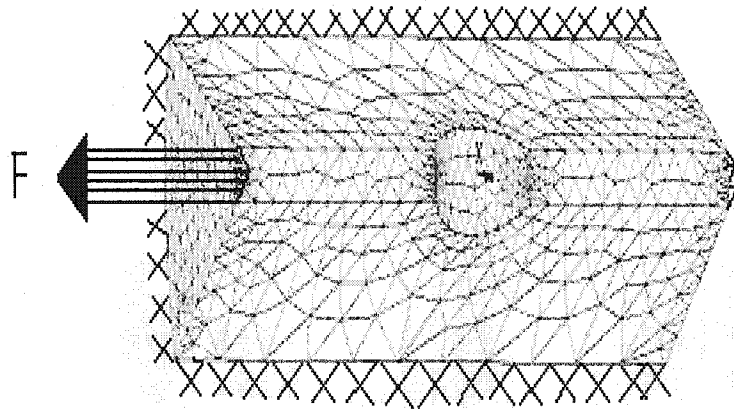
Figure 4.1   **Boundary conditions and loading conditions applied on the FRP rebar with lobe reinforced concrete model**

The analyses of circular-shaped lobes on the FRP rebar reinforced concrete model include studies on different radii of the circular-shaped lobe. Dimensions of the models studied are shown in Table 4.1.

Table 4.1 Dimensions of FRP rebar with circular-shaped lobe reinforced concrete models

	Dimension
Length of concrete	110mm
Radius of concrete	33mm
FRP rebar length	110mm
Lobe radius R of Model #1	9mm
Lobe radius R of Model #2	10mm
Lobe radius R of Model #3	11mm
Lobe radius R of Model #4	12mm
Lobe radius R of Model #5	13mm

ANSYS results of the circular-shaped lobe of radius 11mm are shown in Figures 4.2 and 4.3. Longitudinal stresses distributed inside the concrete and the FRP rebar are shown separately.
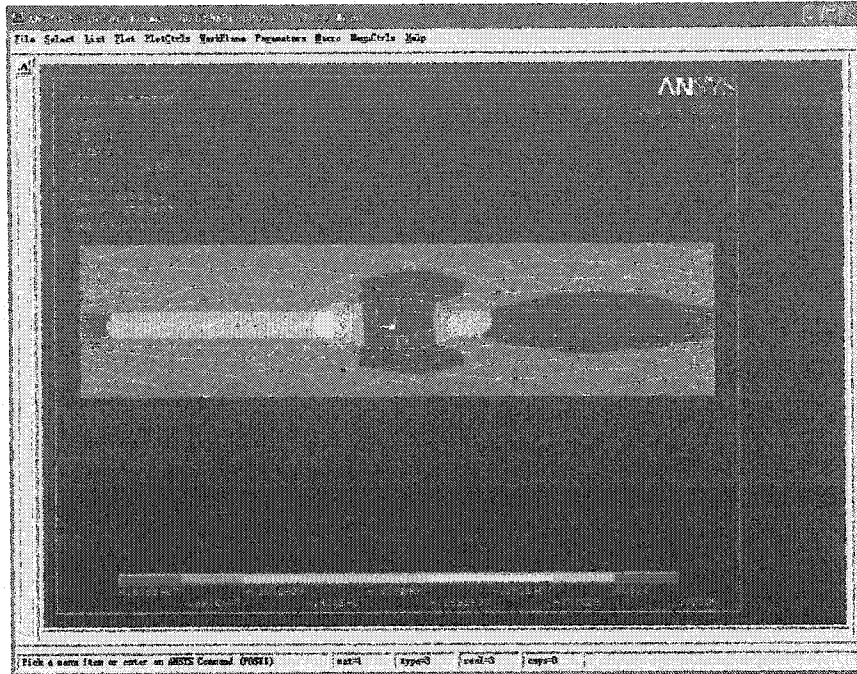
Figure 4.2   Longitudinal stress distribution in concrete with

radius of 11mm circular-shaped lobe
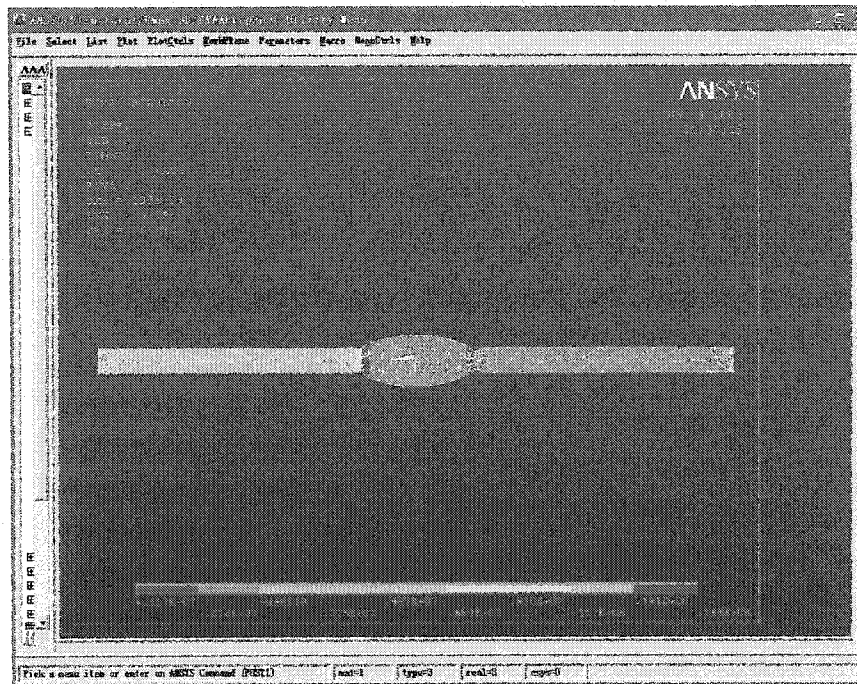
Figure 4.3   Longitudinal stress distribution in FRP rebar with

radius of 11mm circular-shaped lobe

To compare the normal stresses and shear stresses along each direction of the model, one group of nodes were chosen on the interface of the concrete and FRP rebar along the longitudinal direction, The stress values on each nodes are shown in Figures 4.4 and 4.5.
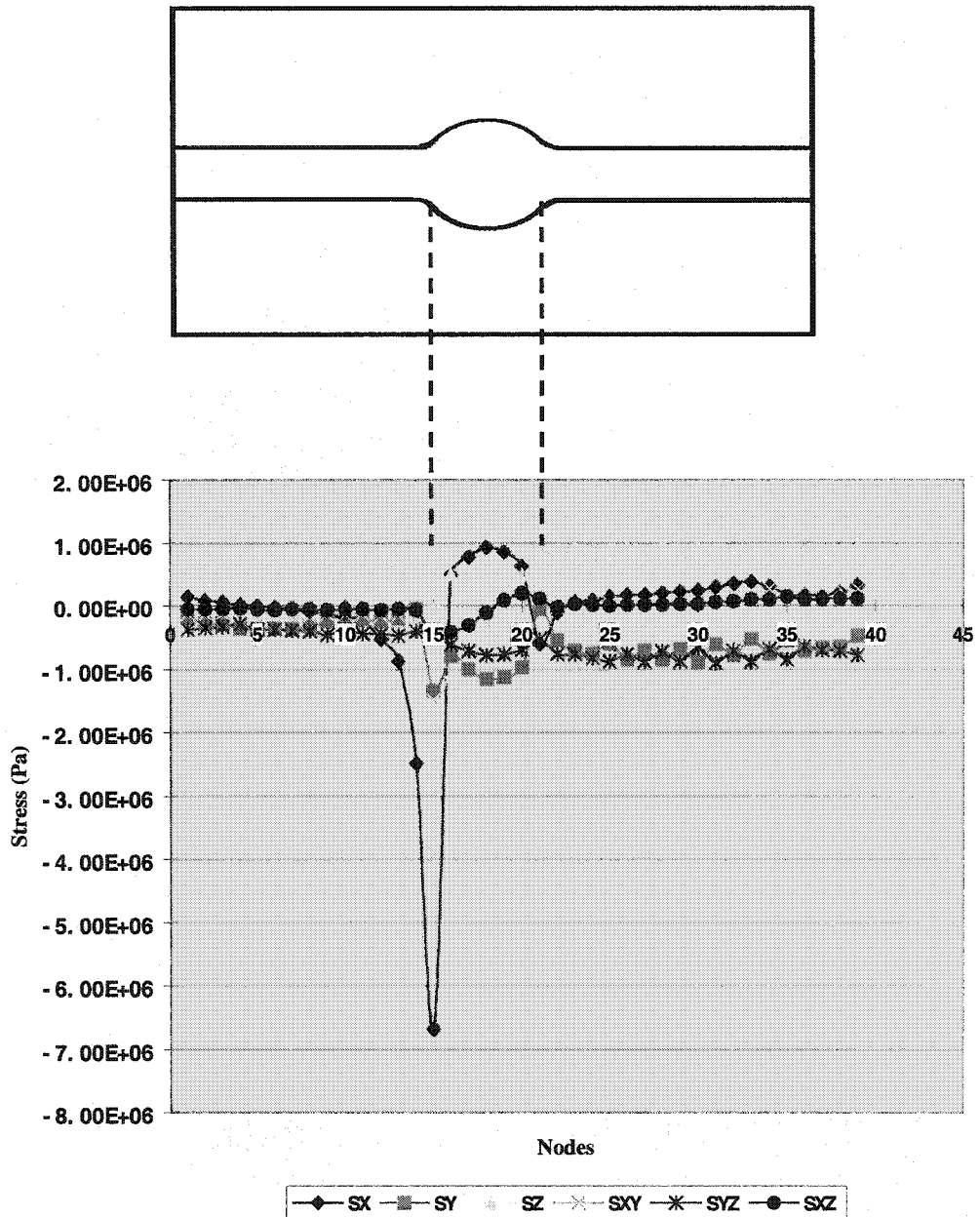
Figure 4.4   Stress at the interface distribution of radius of 11mm

circular-shaped lobe embedded in concrete

Figure 4.4 shows the X, Y, Z direction stresses and XY, YZ, XZ shear stresses in the concrete. The X direction stress is the largest among the all six stresses. It is because the force is applied along the longitudinal (X) direction of the FRP rebar. Also it was found that the peak of X direction stress is not at the middle of the model but on the left side of the lobe. It is because when the FRP rebar pulled, the left part of concrete that is close to the lobe was compressed.
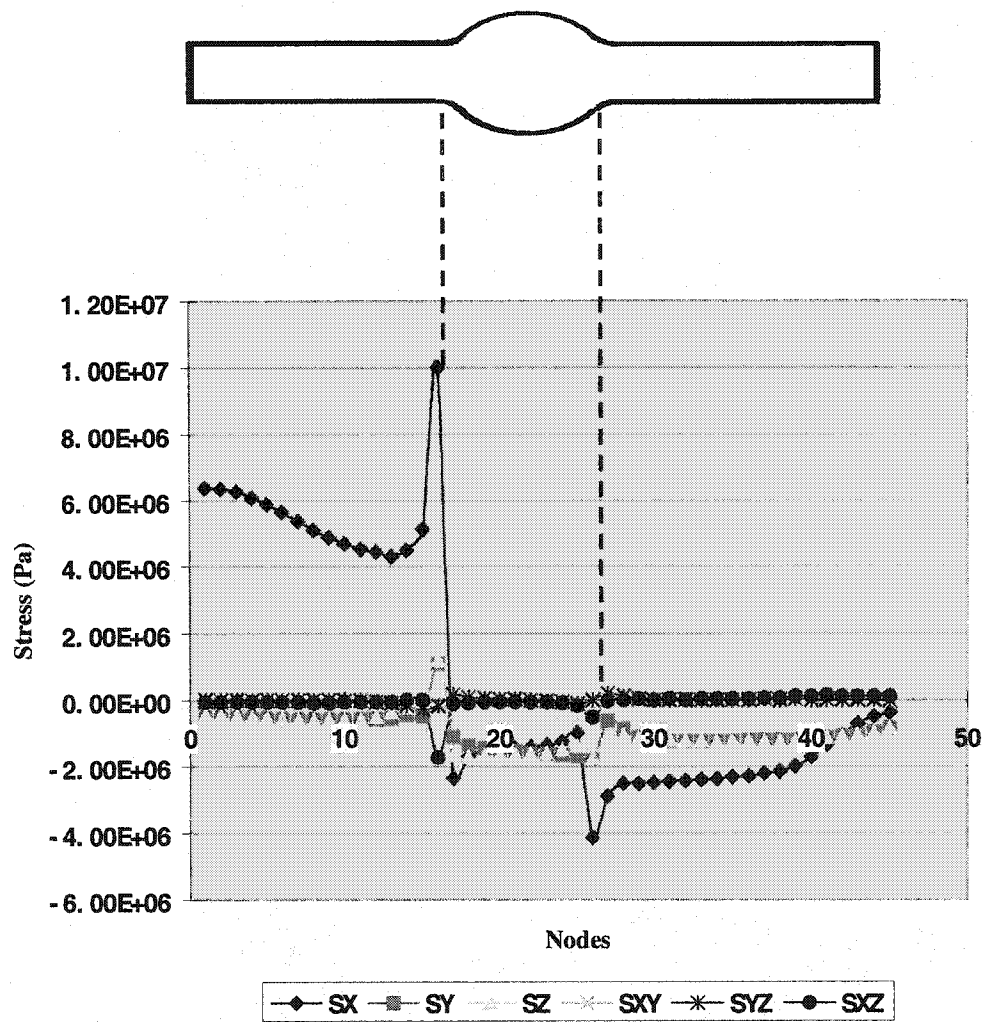
Figure 4.5   **FRP rebar stress distribution of radius of 11mm**

circular-shaped lobe embeded in concrete

Figure 4.5 show the X, Y, Z direction stresses and XY, YZ, XZ shear stresses in the FRP rebar. It is found that the stress in X direction has the largest value. This largest value is different from the largest value in concrete in that the stress in X direction of FRP rebar has the positive maximum value while the stress in concrete has the negative value. This is reasonable because FRP rebar was pulled in the analysis. So its tensile stress must be high. The concrete prevents the FRP rebar from being pulled out, so, the left part of the concrete shows the negative (Compressive) stresses. The critical stresses in concrete with the lobe of radius of 11mm are shown in Table 4.2.

Table 4.2   Critical stresses in concrete with the lobe of radius of 11mm

	SX (MPa)	SY (MPa)	SZ (MPa)	SXY (MPa)	SYZ (MPa)	SXZ (MPa)
Minimum values						
Node	3863	3032	2076	4177	2571	4173
Value	-6.77	-1.47	-3.58	-2.17	-1.17	-1.80
Maximum values						
Node	2555	4006	4182	3038	3436	2082
Value	0.93	0.55	1.42	0.77	0.065	0.53

Negative values in Table 4.2 refer to the compressive stresses and positive values refer to the tensile stresses. Because concrete is an isotropic material, the value with largest amplitude (Negative values were considered only) among the minimum values of SX, SY, SZ was chosen to be compared with the compressive strength of the

54

concrete for failure consideration. Also, the largest value (Positive values were considered only) among the maximum values of SX, SY, SZ was chosen to be compared with the tensile strength of the concrete for same. However for the shear stress, no matter whether the value is negative or positive it makes no difference when checking whether the structure will fail or not. So the largest value (Ignore the positive or negative symbol) among maximum values and minimum values of SXY, SYZ, SXZ was chosen to compare with the shear strength of the concrete to check if the concrete fails or not.

Following the rule explained above, Table 4.3 lists the ratio of stress/strength of concrete when lobe radius is 11mm.

Table 4.3   Ratio between the Stress and Strength of concrete when lobe radius is 11mm

Tensile strength (MPa)	3.15	Maximum Tensile stress	1.42 *(Node 4182)*	Stress / strength	45%
Compressive strength (MPa)	27.50	Maximum Compressive stress	6.77 *(Node 3863)*	Stress / strength	25%
Shear strength (MPa)	3.10	Maximum Shear stress	2.17 *(Node 4177)*	Stress / strength	70%

Figure 4.6 shows the locations where critical stresses exist. Figure 4.7 illustrates the node number where critical stresses occur.
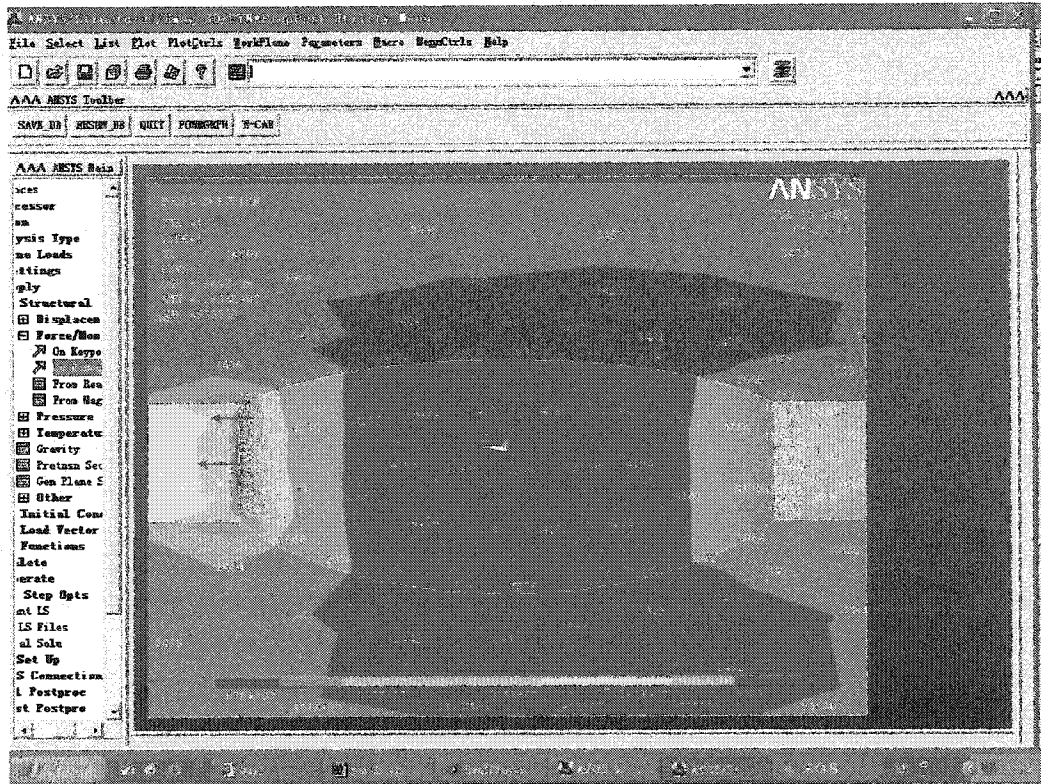
Figure 4.6   Locations of critical stresses
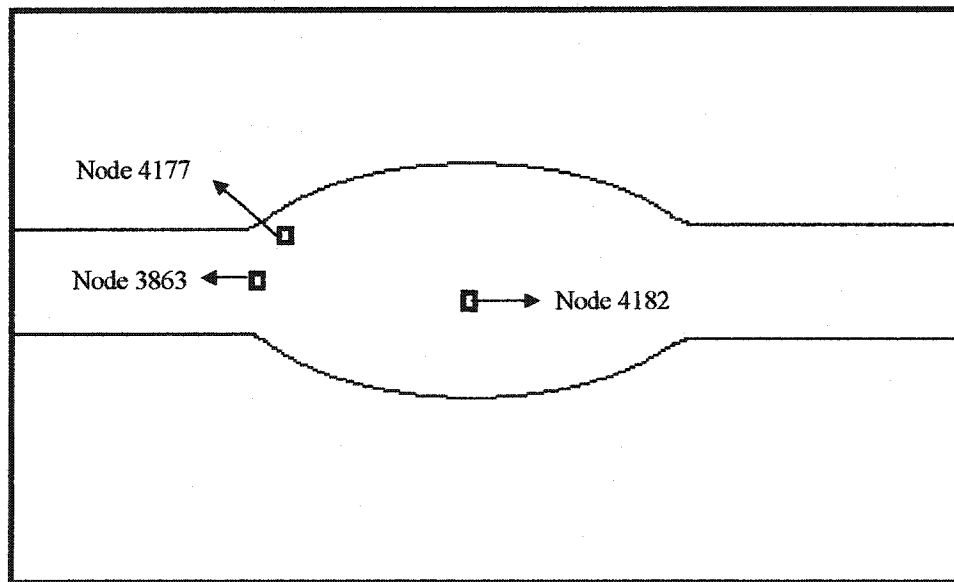
Node 4177 --- Maximum shear stress (2.17MPa)

Node 3863 --- Maximum compressive stress (6.77MPa)

Node 4182 --- Maximum tensile stress (1.42MPa)

Figure 4.7   Node number where critical stresses occur in concrete

Table 4.4 lists the ratios of stress/strength in FRP rebar when lobe radius is 11mm.

Table 4.4   Ratio between the Stress and Strength of FRP rebar when lobe radius is 11mm

Tensile strength (MPa)	SX	972.6	Maximum Tensile stress (MPa)	SX	10.56	Stress / strength	SX	1.1%
	SY	28.98		SY	1.60		SY	5.5%
	SZ	28.98		SZ	1.36		SZ	4.7%
Shear strength (MPa)	SXY	19.98	Maximum Tensile stress (MPa)	SXY	0.34	Stress / strength	SXY	1.7%
	SYZ	12.3		SYZ	0.53		SYZ	4.3%
	SXZ	12.3		SXZ	0.86		SXZ	7.0%

Compared with the ratios between the stress and strength of concrete, the ratios between the stress and strength of FRP rebar are small. So this means the concrete is more likely to fail before the FRP rebar. Therefore only concrete will be considered in the optimal analysis.

Calculations were performed on other models with different lobe radii. Table 4.5 shows maximum tensile stress, maximum compressive stress and maximum shear stress in concrete for the five models.

Table 4.5 Maximum stresses in concrete of 5 models of FRP rebar with circular

shaped lobe

	CONCRETE Maximum Tensile stress (MPa)	CONCRETE Maximum Compressive stress (MPa)	CONCRETE Maximum Shear stress (MPa)
Lobe radius of FRP rebar = 9mm	1.46	7.96	4.65
Lobe radius of FRP rebar = 10mm	1.43	8.11	2.21
Lobe radius of FRP rebar = 11mm	1.42	6.77	2.17
Lobe radius of FRP rebar = 12mm	1.44	7.16	2.25
Lobe radius of FRP rebar = 13mm	1.44	7.72	2.19

Using values in Table 4.5, stress / strength ratios of 5 models are shown in Table 4.6.

Table 4.6 Stress/Strength ratios in concrete of 5 models of FRP rebar with

circular-shaped lobe

	Concrete Tensile strength (MPa)	Concrete Compressive strength (MPa)	Concrete Shear strength (MPa)
Strength	3.15	27.50	3.10
Stress/ strength ratio	Maximum Tensile stress / Tensile strength	Maximum Compressive stress / Compressive strength	Maximum Shear stress / Shear strength
Lobe radius of FRP rebar = 9mm	46.3%	28.9%	117.7%
Lobe radius of FRP rebar = 10mm	45.4%	29.4%	71.2%
Lobe radius of FRP rebar = 11mm	45.0%	24.6%	70.0%
Lobe radius of FRP rebar = 12mm	45.7%	26.0%	72.5%
Lobe radius of FRP rebar = 13mm	45.7%	28.0%	70.6%

Figure 4.8 shows the comparison chart of stress/strength ratio of the 5 models.
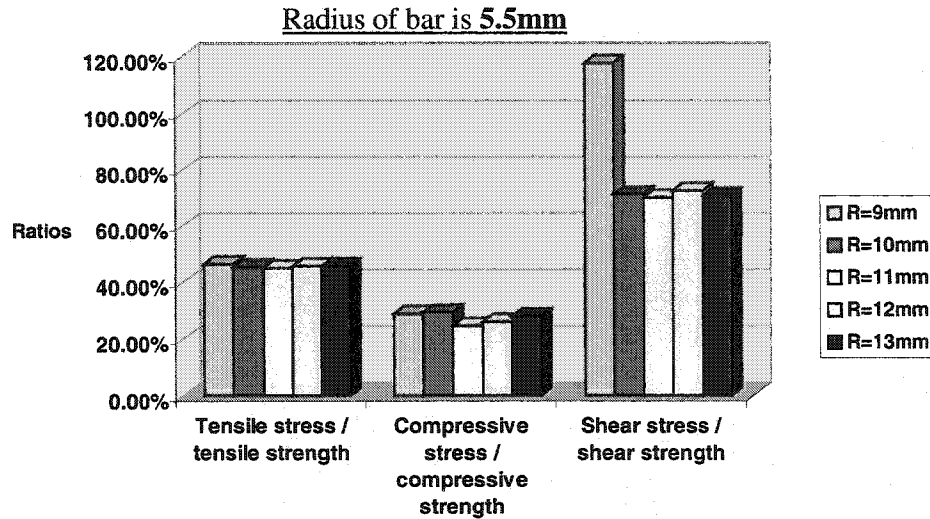
Figure 4.8   Chart of Stress/Strength ratios comparison in concrete of 5 models

for FRP rebar with circular-shaped lobe

According to Figure 4.8, when radius of the lobe is 9mm, the ratio of shear stress /

shear strength exceeds 100%, which means the concrete failed under this dimension.

This may imply that the radius is too small so that slipping occurs.

Also notice from Figure 4.8, that the model of lobe R=11mm always has smaller

ratios than the other four in tensile stress / tensile strength ratio, compressive stress /

compressive strength ratio and shear stress / shear strength ratio. This means that

when the radius of the FRP rebar is 5.5mm, and the circular-shaped lobe radius is

11mm, an optimal condition is obtained.

As such, the optimal case is when the ratio of the lobe radius over rod radius is

$$\frac{R}{r} = \frac{11}{5.5} = 2$$

Verification of the optimal ratio for other dimensions of sample

To check the above optimal ratio two groups of new models were examined. In those two groups of models the radii of the FRP rebars were changed from 5.5mm to 6mm and to 6.5mm respectively. FRP rebar length, concrete length and concrete diameter were also changed proportionately. Five models that have the lobe radius of 9mm, 10mm, 11mm, 12mm and 13mm respectively also were changed according to the changed ratio of diameter of FRP rebar.

Dimensions of the first new group of models are listed in Table 4.7.

Table 4.7 Dimensions of the first new group of models

	Original dimension	Changing ratio	New dimension
Radius of FRP rebar	5.5mm	6 / 5.5	6mm
Radius of concrete	33mm	6 / 5.5	36mm
FRP rebar length	110mm	1/1	110mm
Concrete length	110mm	1/1	110mm
Lobe radius of FRP rebar	9mm	6 / 5.5	9.8mm
Lobe radius of FRP rebar	10mm	6 / 5.5	10.9mm
Lobe radius of FRP rebar	11mm	6 / 5.5	12mm
Lobe radius of FRP rebar	12mm	6 / 5.5	13.1mm
Lobe radius of FRP rebar	13mm	6 / 5.5	14.2mm

From ANSYS® solution, ratios between the stress / strength of this first new group of models is listed in Table 4.8.

Table 4.8   Stress/Strength ratios in concrete of first new group of models

	Concrete Tensile strength (MPa)	Concrete Compressive strength (MPa)	Concrete Shear strength (MPa)
Strength	3.15	27.50	3.10
Stress/ strength ratio	Maximum Tensile stress / Tensile strength	Maximum Compressive stress / Compressive strength	Maximum Shear stress / Shear strength
Lobe radius of FRP rebar = 9.8mm	45.4%	36.0%	100.9%
Lobe radius of FRP rebar = 10.9mm	45.4%	30.7%	96.1%
Lobe radius of FRP rebar = 12mm	45.4%	27.7%	63.5%
Lobe radius of FRP rebar = 13.1mm	46.6%	29.2%	70.3%
Lobe radius of FRP rebar = 14.2mm	47.3%	31.3%	71.6%

Using these values in Table 4.8, Figure 4.9 is obtained.
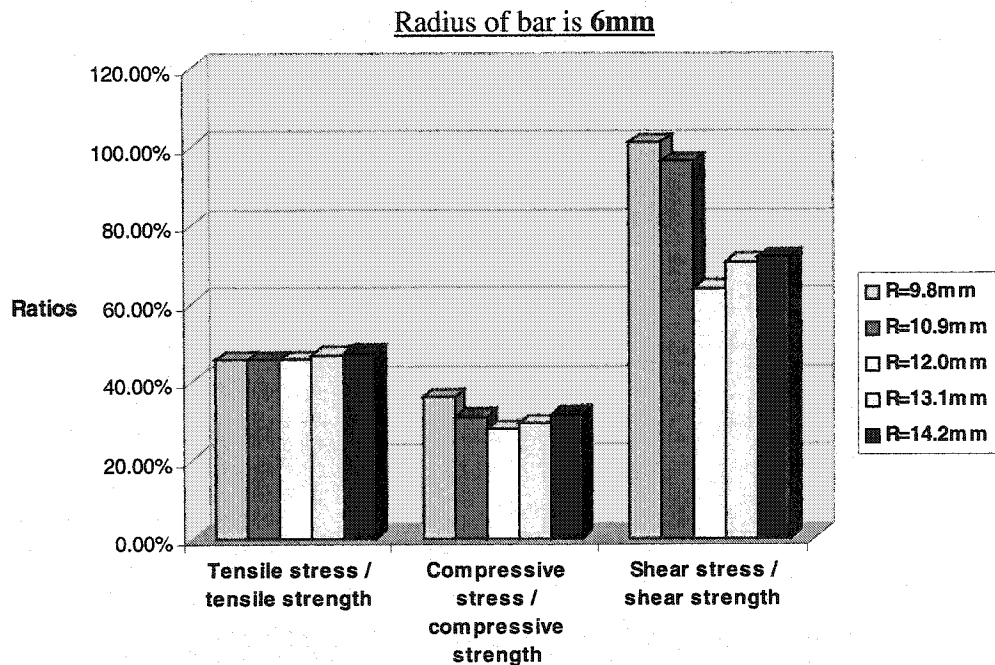
Figure 4.9   Stress/Strength ratios in concrete for 5 models of FRP rebar with circular-shaped lobe and FRP rebar cross-section radius is 6mm

This result shows that when radius of the lobe on FRP rebar is 12mm the ratio is lower.

This means if radius of the circular lobe (R) and the radius of the cross section of FRP rebar (r) follows the relation

$$\frac{R}{r} = \frac{12}{6} = 2$$

the concrete has minimum stresses.

Next, second new group of models were examined. Dimensions of the second group of models are listed in Table 4.9.

Table 4.9   Dimensions of the second new group of models

	Original dimension	Changing ratio	New dimension
Diameter of FRP rebar	5.5mm	6.5 / 5.5	6.5mm
Diameter of concrete	33mm	6.5 / 5.5	39mm
FRP rebar length	110mm	1	110mm
Concrete length	110mm	1	110mm
Lobe radius of FRP rebar	9mm	6.5 / 5.5	10.6mm
Lobe radius of FRP rebar	10mm	6.5 / 5.5	11.8mm
Lobe radius of FRP rebar	11mm	6.5 / 5.5	13mm
Lobe radius of FRP rebar	12mm	6.5 / 5.5	14.2mm
Lobe radius of FRP rebar	13mm	6.5 / 5.5	15.4mm

From ANSYS® solution, ratios between the stress / strength of the second new group

models are listed in Table 4.10.

Table 4.10   Stress/Strength ratios in concrete of the second new group models

	Concrete Tensile strength (MPa)	Concrete Compressive strength (MPa)	Concrete Shear strength (MPa)
Strength	3.15	27.50	3.10
Stress/ strength ratio	Maximum Tensile stress / Tensile strength	Maximum Compressive stress / Compressive strength	Maximum Shear stress / Shear strength
Lobe radius of FRP rebar = 10.6mm	45.8%	39.8%	120.9%
Lobe radius of FRP rebar = 11.8mm	46.1%	37.3%	71.2%
Lobe radius of FRP rebar = 13mm	45.5%	28.7%	69.6%
Lobe radius of FRP rebar = 14.2mm	48.4%	35.2%	77.1%
Lobe radius of FRP rebar = 15.4mm	48.6%	35.4%	77.7%

Figure 4.10 shows the graphic representation of values in Table 4.10.
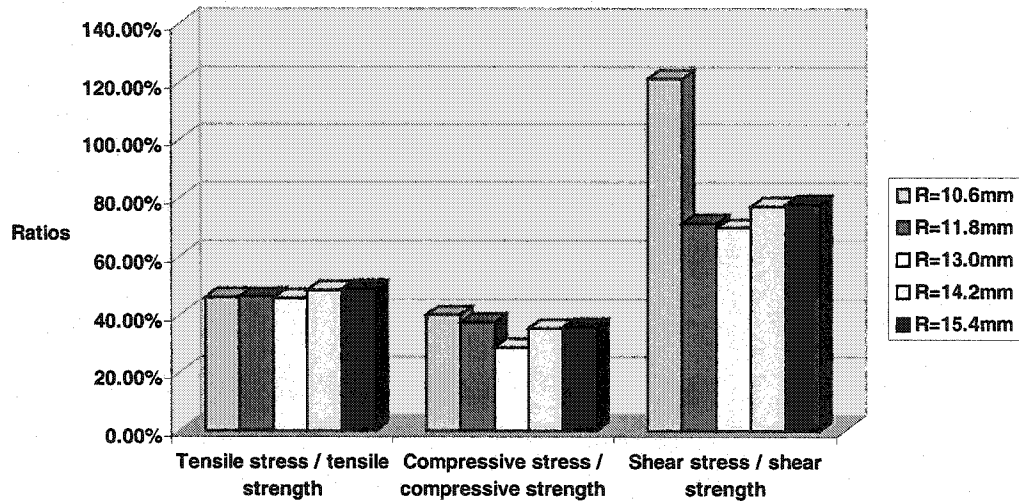
Figure 4.10   **Stress/Strength ratios in concrete of 5 models of FRP rebar with circular-shaped lobe and FRP rebar cross-section radius is 6.5mm**

It can be seen that when radius of the lobe on FRP rebar is 13mm the stresses in the concrete are the lowest.

So best case is the ratio of the lobe radius over rod radius is

$$\frac{R}{r} = \frac{13}{6.5} = 2$$

4.2 Determination of distance between two lobes on the FRP rebars with circular-shaped lobes

The distance L (as shown in Figure 4.11) between the lobes along the FRP rebar is one of interest. The concrete/FRP rebar with 11mm radius lobe was considered. This is because it is the best case in FRP rebar with circular-shaped lobe reinforced concrete system. Figure 4.12 shows the stress distribution curves in the concrete for this model.
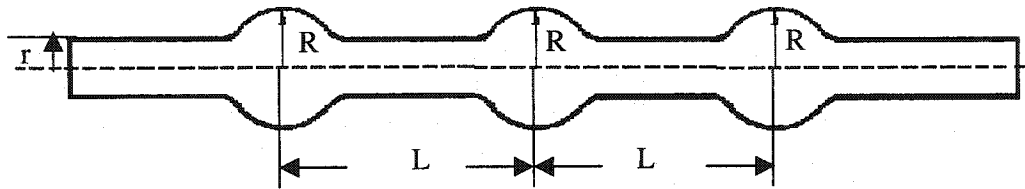
Figure 4.11   Distance between lobes along FRP rebar
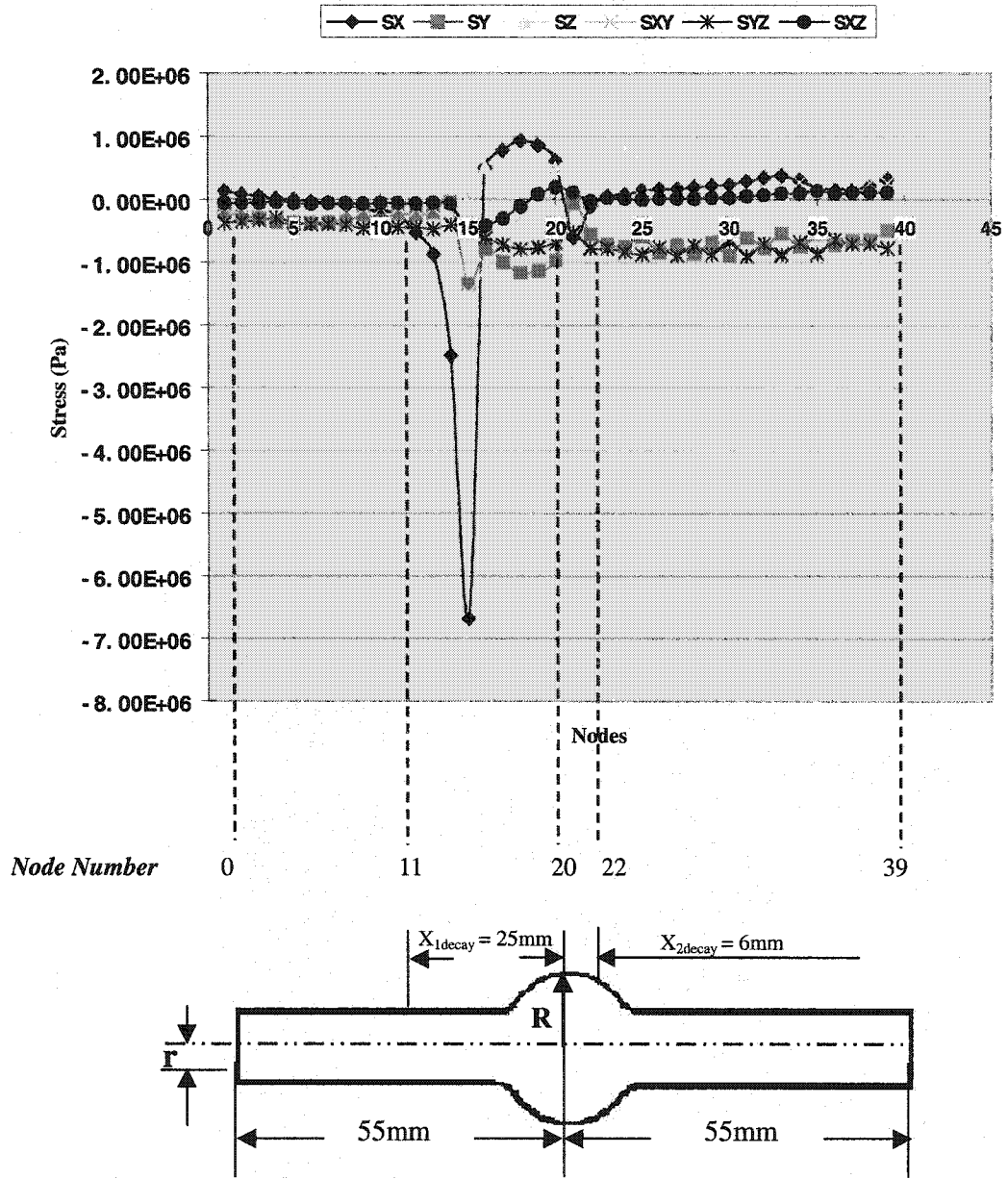
Figure 4.12　　　Illustration of distance between two circular-shaped lobes on

FRP rebar

Referring to the concrete stress distribution above it can be seen that the X direction

stress is much larger compared with the other stresses in the figure. The X direction

maximum stress is 6.8 MPa, and it dies off as one moves away from both sides of the

lobe. In Figure 4.12 stresses are dieing off from node 20 to node 11 on left side and from node 20 to node 22 on right side. So if there is another lobe along the FRP rebar, it can be placed in the area that stresses have died off. The distance for stress decay can be used as a good determination between the lobes.

As illustrated in Figure 4.12,

X_{1decay} = 25mm,

X_{2decay} = 6mm,

Half length of the FRP rebar is 55mm,

Radius of FRP rebar r = 5.5mm and

Radius of the circular-shaped lobe is 11mm.

According to these dimensions a safe distance between the two circular-shaped lobes center L should be

$$(X_{1decay} * 2) \text{ mm} = 50\text{mm}. \quad (\text{For } X_{1decay} > X_{2decay})$$

Where,

X_{1decay} - Distance of stress decay on left side of the lobe

X_{2decay} - Distance of stress decay on right side of the lobe

L - Distance between two lobe centers

From the above result, the optimal ratio for the different dimensions can be:

$$r / R / L = 5.5 / 11 / 50 = 1 / 2 / 9$$

4.3   Distance between two FRP rebars with circular-shaped lobes

Another parameter of interest in the design of optimal coefficient for the reinforcement system is the radial distance between the rebars (As shown in Figure 4.13). This distance can be larger for rebar with lobes than for straight rebars.
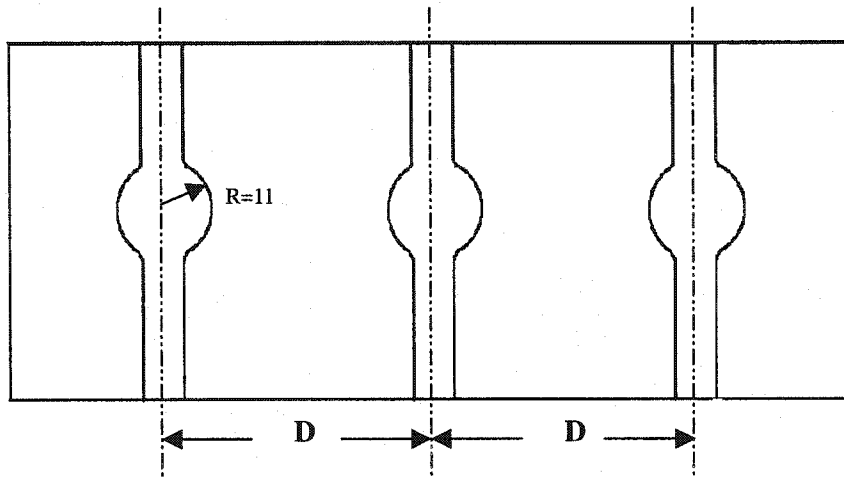
Figure 4.13   **Distance between the two FRP rebars**

(For circular-shaped model)

The concrete/FRP rebar with the circular-shaped lobe system (R = 11mm) is considered. Figure 4.14 shows the stress distribution in the concrete.
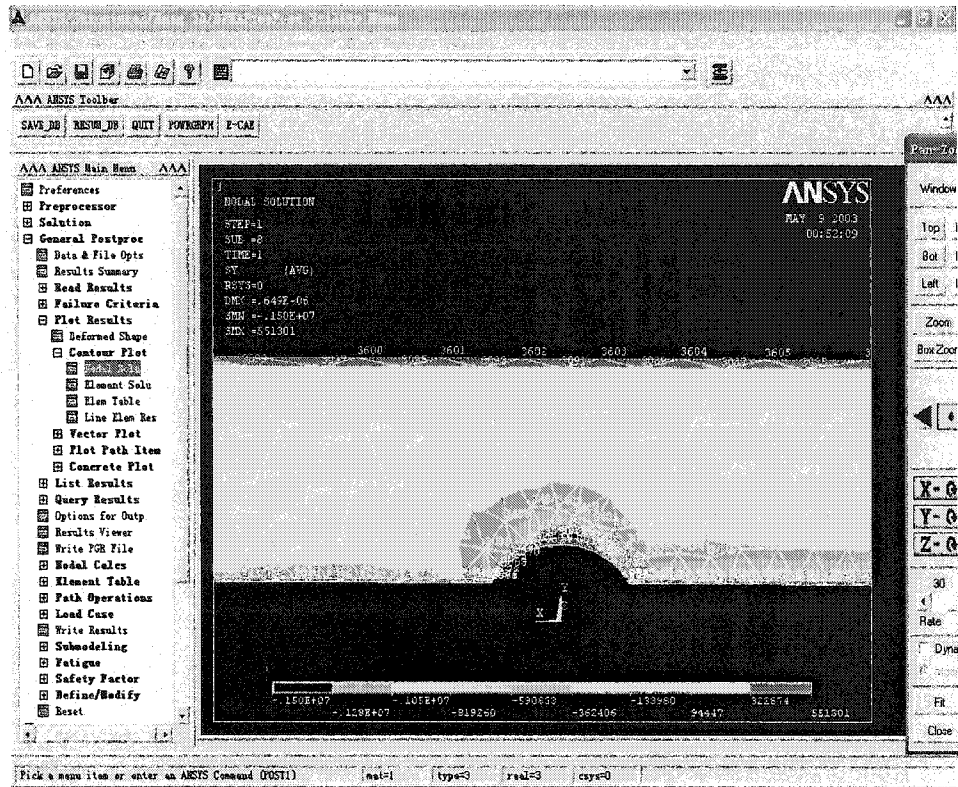
Figure 4.14   **Concrete stress distribution with FRP rebar with**

R = 11mm circular-shaped lobe

The stress decay in the direction perpendicular to the bar is examined. Five groups of

nodes are examined. Figure 4.15 illustrates the location of the 5 groups of nodes.
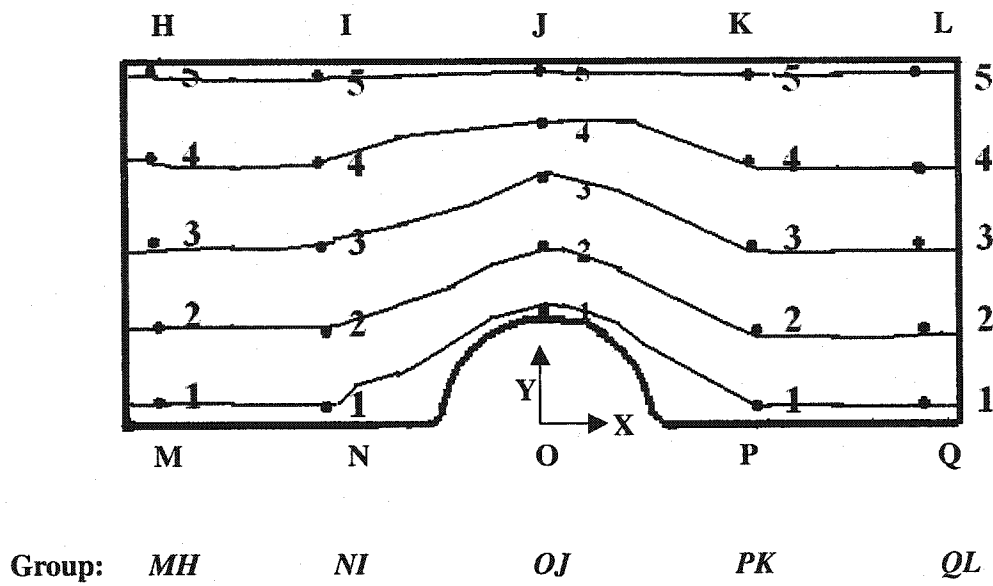
Figure 4.15   **5 groups of nodes in the concrete along the radial direction in circular-shaped lobe model**

A chart of the first group of nodes stress distribution along the radial direction in concrete is shown in Figure 4.16. This figure also illustrates how the stress distribution corresponds with the group of nodes in the concrete.
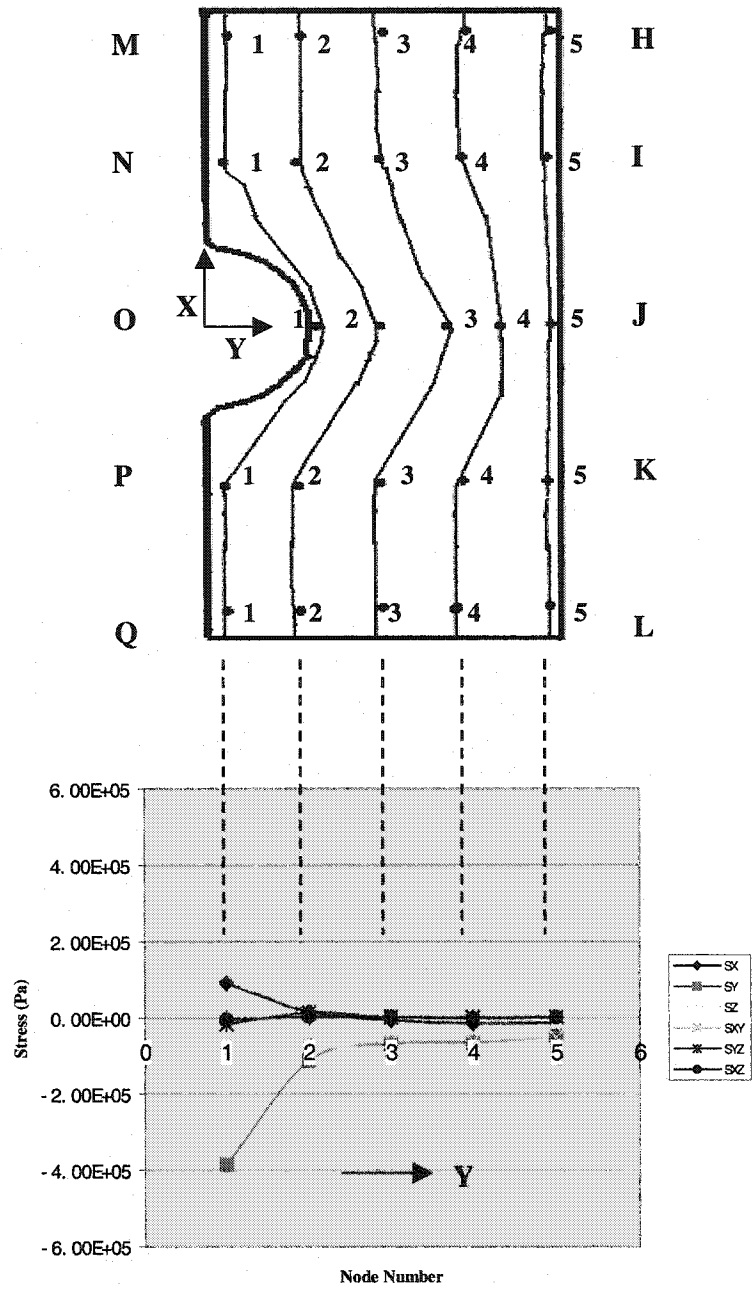
Figure 4.16 **Concrete stress distribution along the radial direction for nodes group MH (Circular-shaped lobe model)**

According to the 5 groups of nodes, stress distribution along the radial direction in concrete are shown in Figure 4.16 to Figure 4.20.
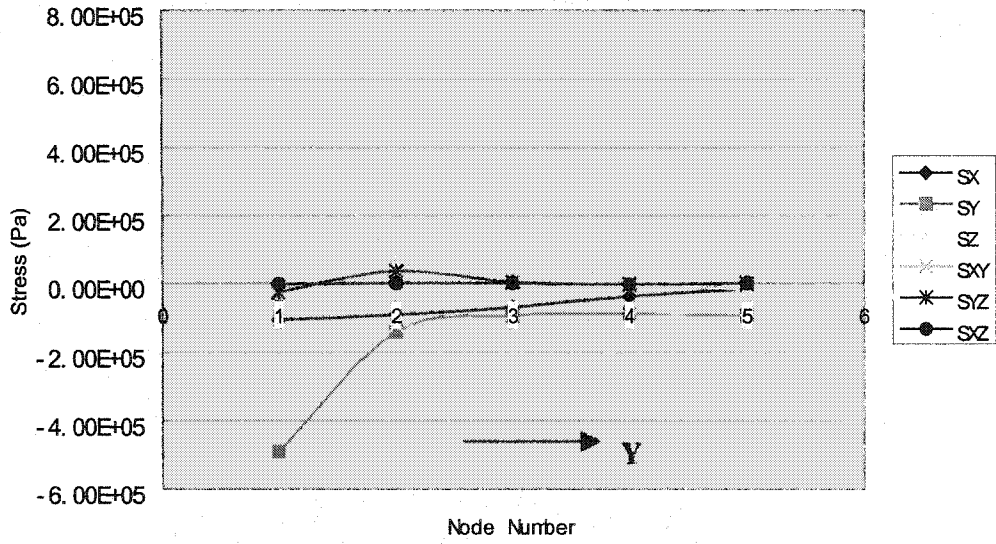
Figure 4.17   **Concrete stress distribution along the radial direction for nodes**

group NI (Circular-shaped lobe model)
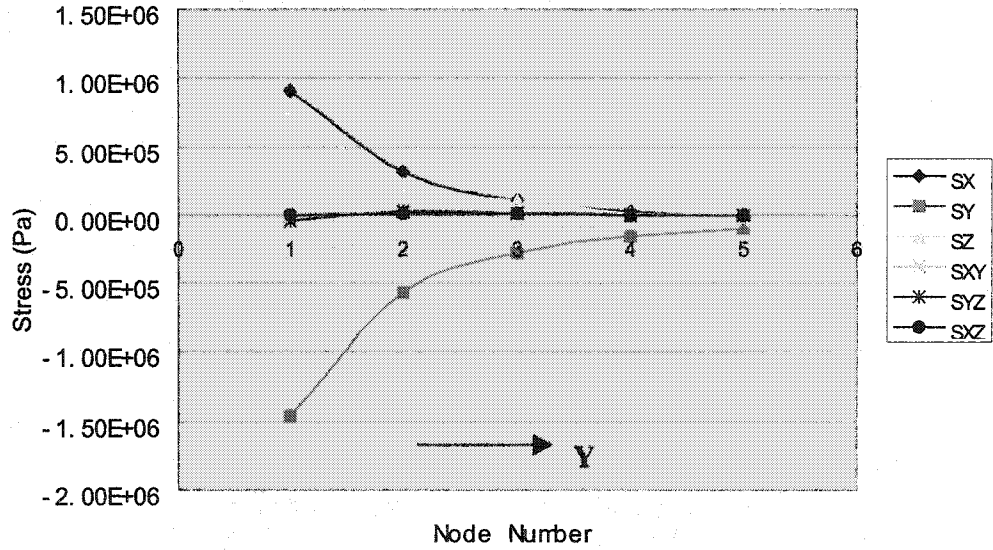
Figure 4.18   **Concrete stress distribution along the radial direction for nodes**

group OJ (Circular-shaped lobe model)
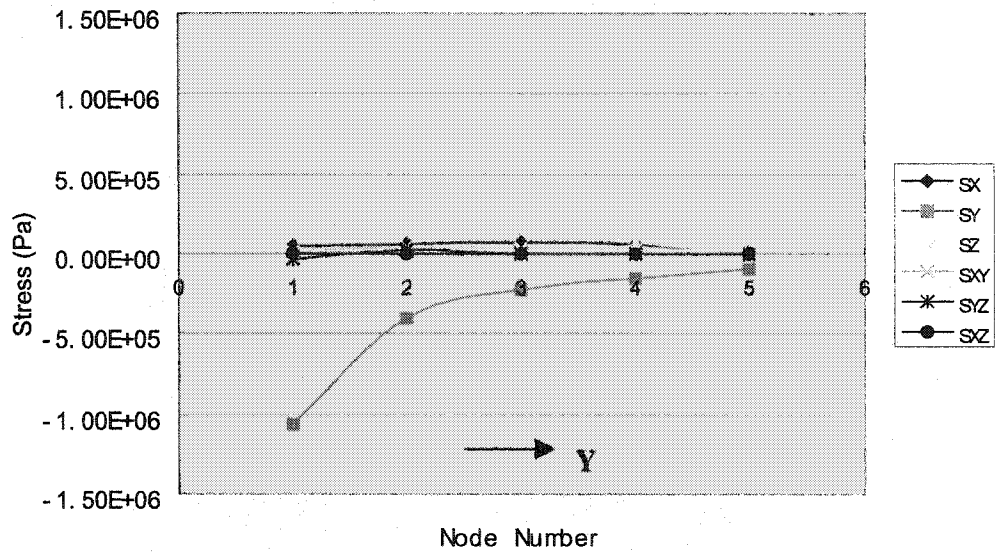
Figure 4.19   **Concrete stress distribution along the radial direction for nodes**

group PK (Circular-shaped lobe model)
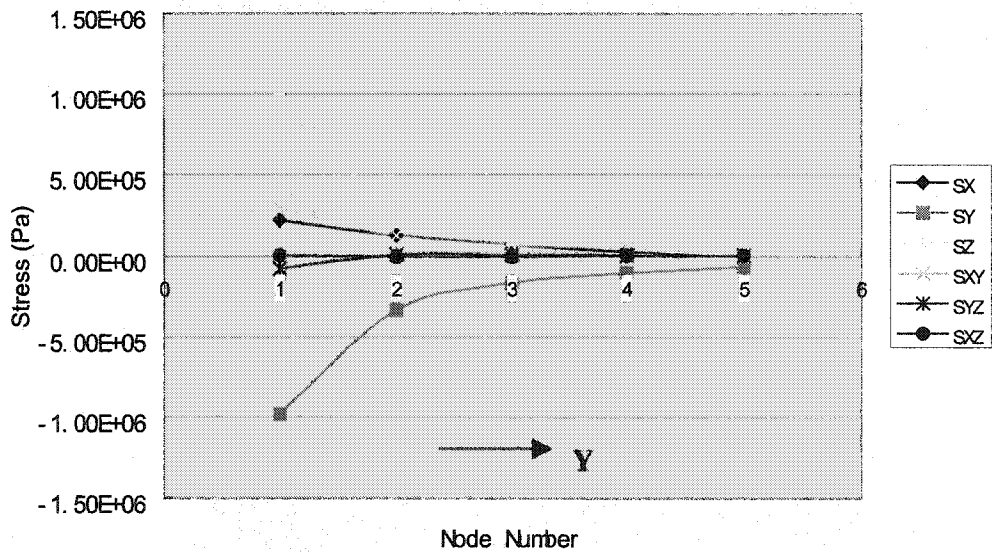
Figure 4.20   **Concrete stress distribution along the radial direction for nodes**

group QL (Circular-shaped lobe model)

From the figures above, it can be seen that from node 1 to 3 stresses have died off (Distance BD). The nodes group QL is used to give the distance guide between the two FRP rebars in the concrete system.
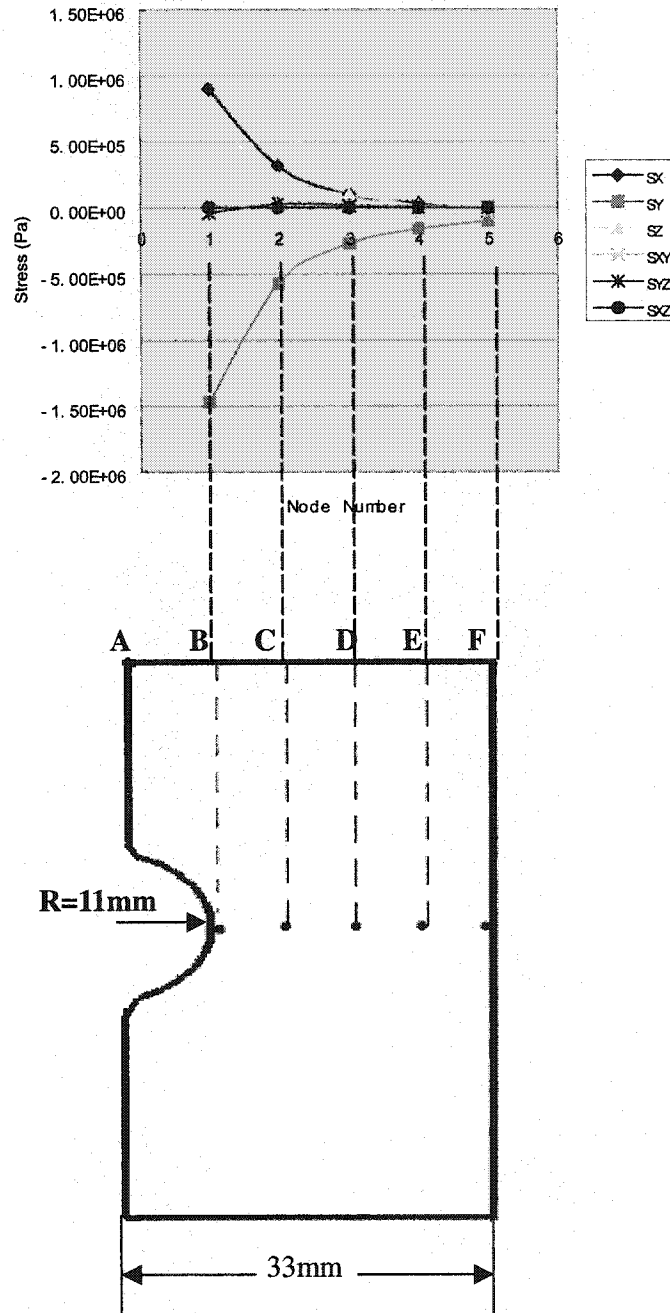
Figure 4.21   Stress distribution corresponding with the nodes group OJ on the concrete of circular-shaped lobe model

According to the dimensions given in Figure 4.21,

Distance between each node is the same BC = CD = DE = EF,

Radius of the concrete is AF = 33mm,

Radius of the circular-shaped lobe is R = 11mm,

BD = ((33mm − R) / 4)*2 = 11mm,

So the distance between two FRP rebars in the concrete should be

2 * (BD + R) = 44mm

Figure 4.22 shows that if the radius of FRP rebar is 5.5mm, distance between two circular-shaped lobes FRP rebars should be 44mm.
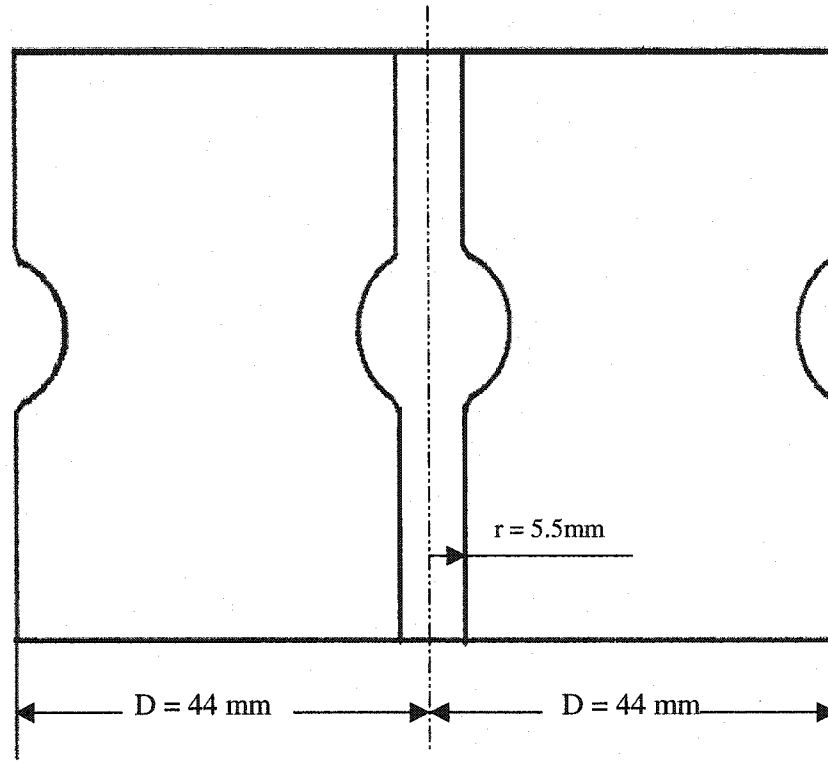
Figure 4.22   **Distance between two FRP rebars in the concrete of circular-shaped lobe model**

From this it can be considered that:

For FRP rebar with circular-shaped lobe,

Radius of the FRP rebar cross section is r,

Distance between the two FRP rebars with circular-shaped lobes is D,

Then the ratio should be:

$$r / D = 5.5 / 44 = 1 / 8$$

Summarize the optimal ratio, relations between the parameters in terms of FRP rebar

(With circular-shaped lobe) radius r are as follows, (As shown in the Figure 4.23)

If FRP rebar with circular-shaped lobe,

Radius of the FRP rebar cross section is r,

Radius of circular-shaped lobe is R,

Distance between the two FRP rebars with circular-shaped lobes is D,

Distance between the two lobes along FRP rebars (With circular-shaped lobes) is L,

then the following is the optimal ratio

$$r / R / L / D = 5.5 / 11 / 50 / 44 = 1 / 2 / 9 / 8$$
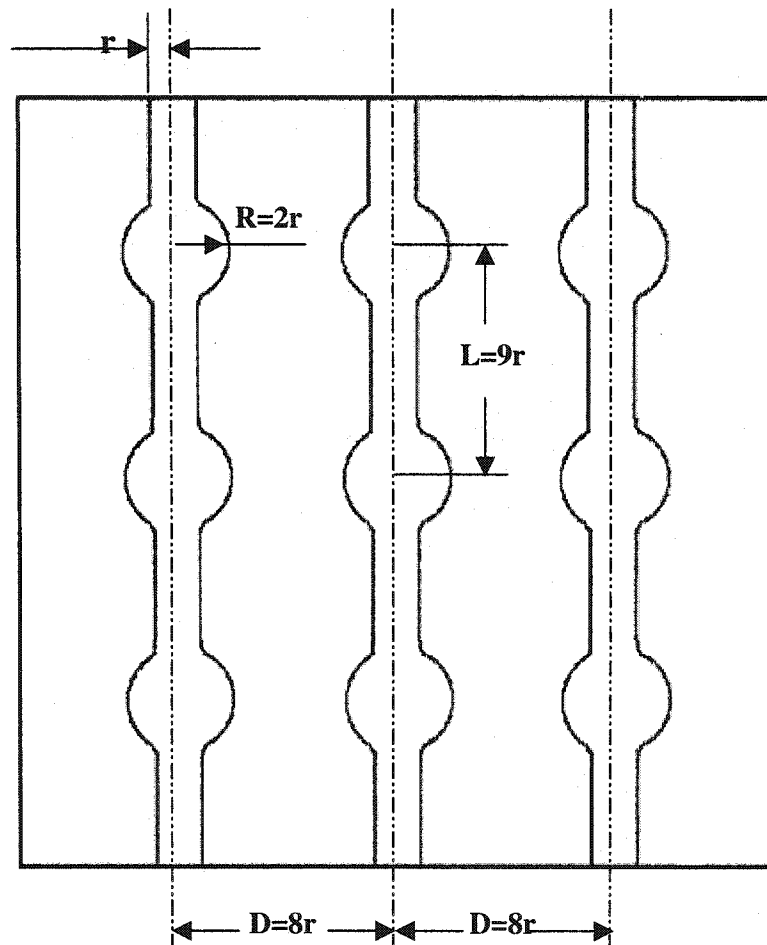
Figure 4.23   **Optimal ratio of r, R, L and D**

Note that the above configuration is for rebars with identical spacing configuration and distance between them is the maximum. If one wants to mesh the rebar as shown in Figure 4.24, then the distance between the rebars can be less than what is shown above.
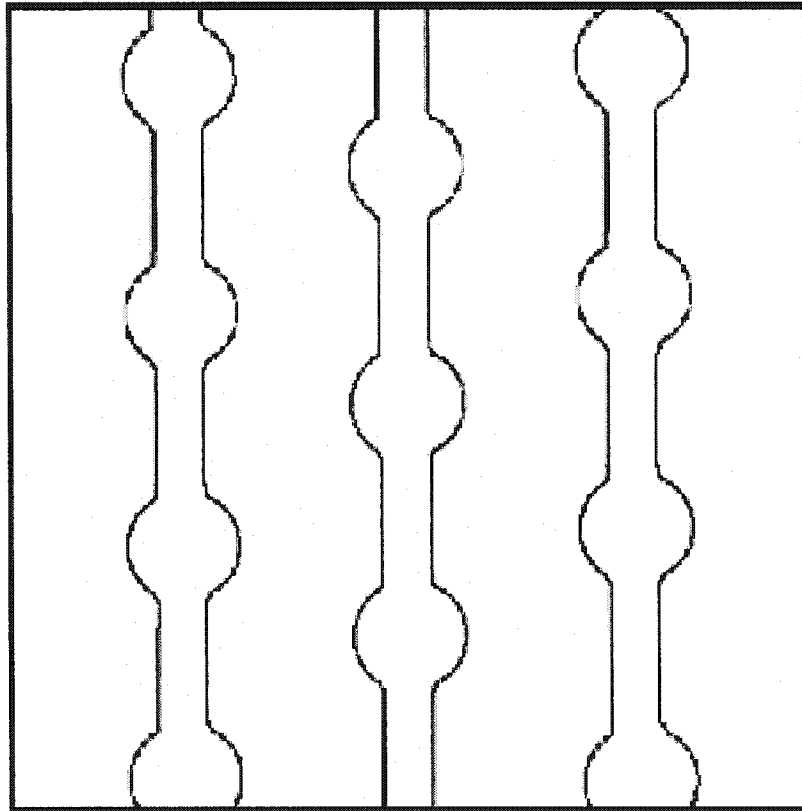
Figure 4.24   Circular-shaped rebar with mashed spacing

4.4   Rebar of fixed length, fixed diameter and elliptical-shaped lobe

Determination of optimal aspect ratio of lobe (Case 2)

Introduction

Compared with the circular-shaped lobe, the elliptical-shaped lobe theoretically should offer a gentler joint interface for the FRP rebar.

According to the conclusion obtained in Chapter 3, if the radius of the circular lobe (R) and the radius of the cross section of FRP rebar (r) have the ratio of

$$\frac{R}{r} = 2$$
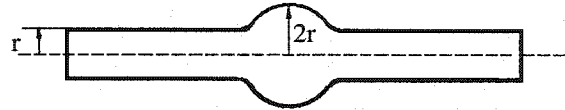
the reinforcement system is optimal.

So, for optimization of the elliptical-shaped lobe models, one can start with a ratio of R/b = 2 and change the dimension of the major radius of the lobe. (*b* — minor radius, *a* — major radius)

Because the optimized dimension of the radius of the circular-shaped lobe was 11mm, the minor radius of the elliptical-shaped lobe was set at 11mm. The first model is with the major radius of 12mm and the last elliptical-shaped lobe model has the major

radius of 22mm, which is twice the minor radius. So, elliptical-shaped lobe models with major radii of 12mm, 13mm, 14mm, 15mm, 16mm, 17mm, 18mm, 19mm, 20mm, 21mm and 22mm were investigated.

Dimensions of models are shown in Table 4.11.

Table 4.11   Dimensions of elliptical-shaped lobe, concrete and FRP rebars

	Dimension
Length of concrete	110mm
Radius of concrete	33mm
FRP rebar length	110mm
FRP rebar lobe minor radius	5.5mm
Major radius of Model #1	12mm
Major radius of Model #2	13mm
Major radius of Model #3	14mm
Major radius of Model #4	15mm
Major radius of Model #5	16mm
Major radius of Model #6	17mm
Major radius of Model #7	18mm
Major radius of Model #8	19mm
Major radius of Model #9	20mm
Major radius of Model #10	21mm
Major radius of Model #11	22mm

All boundary conditions applied were the same as the circular-shaped models. ANSYS® solution gives the stresses of those models.

Table 4.12 shows maximum tensile stress, maximum compressive stress and maximum shear stress in the concrete for these models.

Table 4.12   Maximum tensile stress, maximum compressive stress and maximum shear stress in concrete of different elliptical-shaped lobe models

	CONCRETE Maximum Tensile stress (MPa)	CONCRETE Maximum Compressive stress (MPa)	CONCRETE Maximum Shear stress (MPa)
Model #1	1.45	6.49	2.47
Model #2	1.43	6.54	2.25
Model #3	1.39	6.02	2.34
Model #4	1.39	6.34	1.94
Model #5	1.42	6.20	2.75
Model #6	1.42	6.14	2.63
Model #7	1.40	5.94	3.09
Model #8	1.38	5.62	2.38
Model #9	1.44	5.82	2.65
Model #10	1.43	6.05	2.49
Model #11	1.43	5.90	2.77

According to Table 4.12, ratios of stress / strength are shown in Table 4.13.

Table 4.13   Ratios of stress / strength of embedded concrete of different

elliptical-shaped lobe models

	Concrete Tensile strength (MPa)	Concrete Compressive strength (MPa)	Concrete Shear strength (MPa)
Strength	3.15	27.50	3.10
Stress/ strength ratio	**Maximum Tensile stress / Tensile strength**	**Maximum Compressive stress / Compressive strength**	**Maximum Shear stress / Shear strength**
Model #1	46.0%	23.6%	79.6%
Model #2	45.3%	23.7%	72.5%
Model #3	44.1%	21.8%	75.4%
Model #4	*44.1%*	*23.0%*	*62.5%*
Model #5	45.0%	22.5%	88.7%
Model #6	45.0%	22.3%	84.8%
Model #7	44.4%	21.6%	99.6%
Model #8	43.8%	20.4%	76.7%
Model #9	45.7%	21.1%	85.4%
Model #10	45.3%	22.0%	80.3%
Model #11	45.3%	21.4%	89.3%

For clarity, recall the Ratios of stress / strength for circular-shaped lobes embedded in

concrete which were shown in Table 4.6.

Table 4.6   Stress/Strength ratios in concrete of 5 models of FRP rebar with

circular-shaped lobe

	Concrete Tensile strength (MPa)	Concrete Compressive strength (MPa)	Concrete Shear strength strength (MPa)
Strength	**3.15**	**27.50**	**3.10**
Stress/ strength ratio	**Maximum Tensile stress / Tensile strength**	**Maximum Compressive stress / Compressive strength**	**Maximum Shear stress / Shear strength**
Lobe radius of FRP rebar = 9mm	**46.3%**	**28.9%**	**117.7%**
Lobe radius of FRP rebar = 10mm	**45.4%**	**29.4%**	**71.2%**
Lobe radius of FRP rebar = 11mm	*45.0%*	*24.6%*	*70.0%*
Lobe radius of FRP rebar = 12mm	**45.7%**	**26.0%**	**72.5%**
Lobe radius of FRP rebar = 13mm	**45.7%**	**28.0%**	**70.6%**

The best case for the circular-shaped lobe models is when radius of the lobe is 11mm; the concrete has the maximum tensile stress/strength ratio of 45.0%, maximum compressive stress ratio of 24.6% and maximum shear ratio of 70.0%. Compared with the ratio listed in Table 4.13 it is observed that under the same conditions all of the models with elliptical-shaped lobe have less compressive stress (Low compressive stress / compressive strength ratio) than the best case of the circular-shaped lobe model. Some of the elliptical-shaped lobe models have less tensile stress than the best case of circular-shaped lobe model, for example, Model #3, Model #4, Model #5, Model #6, Model #7 and Model #8. One of the elliptical-shaped lobe models (Model #4) has less shear stress than the best case of circular-shaped lobe model. In other words, it means under the same conditions models with elliptical-shaped lobes are

84

better than the model with circular-shaped lobe with radius of 11mm (The best case of circular-shaped lobe). So FRP rebar with elliptical-shaped lobes is preferred to be used than the circular-shaped one to reinforced concrete.

Summarizing the analysis above, Model #4 is the best elliptical-shaped lobe model because it has less tensile, compressive and shear stress than the best case of circular-shaped lobe model. Table 4.14 shows the comparison of the two models.

Table 4.14   Stress/Strength ratios in concrete of FRP rebar with circular-shaped lobe and elliptical-shaped lobe

	Concrete Tensile strength (MPa)	Concrete Compressive strength (MPa)	Concrete Shear strength strength (MPa)
Strength	3.15	27.50	3.10
Stress/ strength ratio	Maximum Tensile stress / Tensile strength	Maximum Compressive stress / Compressive strength	Maximum Shear stress / Shear strength
Best case of circular-shaped lobe models (Radius of the lobe = 11mm)	45.0%	24.6%	70.0%
Best case of elliptical-shaped lobe models (Model #4)	44.1%	23.0%	62.5%

Therefore one can conclude that when major radius of elliptical-shaped lobe is 15mm (Model #4), the best elliptical-shaped lobe model is obtained.

Comparison of FRP rebars with circular-shaped lobe, elliptical-shaped lobe and bars

with no lobe (Straight bar) is shown in Table 4.15.

Table 4.15 **Comparison of FRP rebars with circular-shaped lobe,**

elliptical-shaped lobe and bar with no lobe

FRP rebar type		Mechanical interlock (Concrete maximum Shear stress / Shear strength)	Compressive stress in concrete (Concrete Maximum Compressive stress / Compressive strength)
bar without lobe		0%	0%
bar with circular-sh aped lobe		70.0%	24.6%
bar with elliptical-sh aped lobe		62.5%	23.0%

Table 4.15 illustrates that straight FRP rebar easy to fail (Slip out) since it provides no mechanical interlock along the bar. FRP rebars with circular-shaped lobe can provide more mechanical interlock, but concrete can fail easily because of high compressive stress. FRP rebar with elliptical-shaped lobe is a trade-off between the two cases. It provides more mechanical interlock than straight bar so that the bar can not slip out easily. It also produces less compressive stress in concrete than the circular-shaped lobe. Obviously, elliptical-shaped lobe FRP rebar is the optimal model.

Conclusion

If the major radius of the elliptical-shaped lobe is a, minor radius is b,

then, it can be concluded that: when

$$\frac{a}{b} = \frac{15}{11} = 1.36$$

the reinforcement system is optimal.

4.5 Elliptical-shaped lobe interval guide

As in the case of circular-shaped lobe, the distance between the lobes is one important parameter in the design of the rebar. In the previous sections results show that the elliptical-shaped lobe with major radius of 15mm (Model 4) is the best case. So the study of distance between the two lobes of elliptical-shaped lobe will be based on this model.
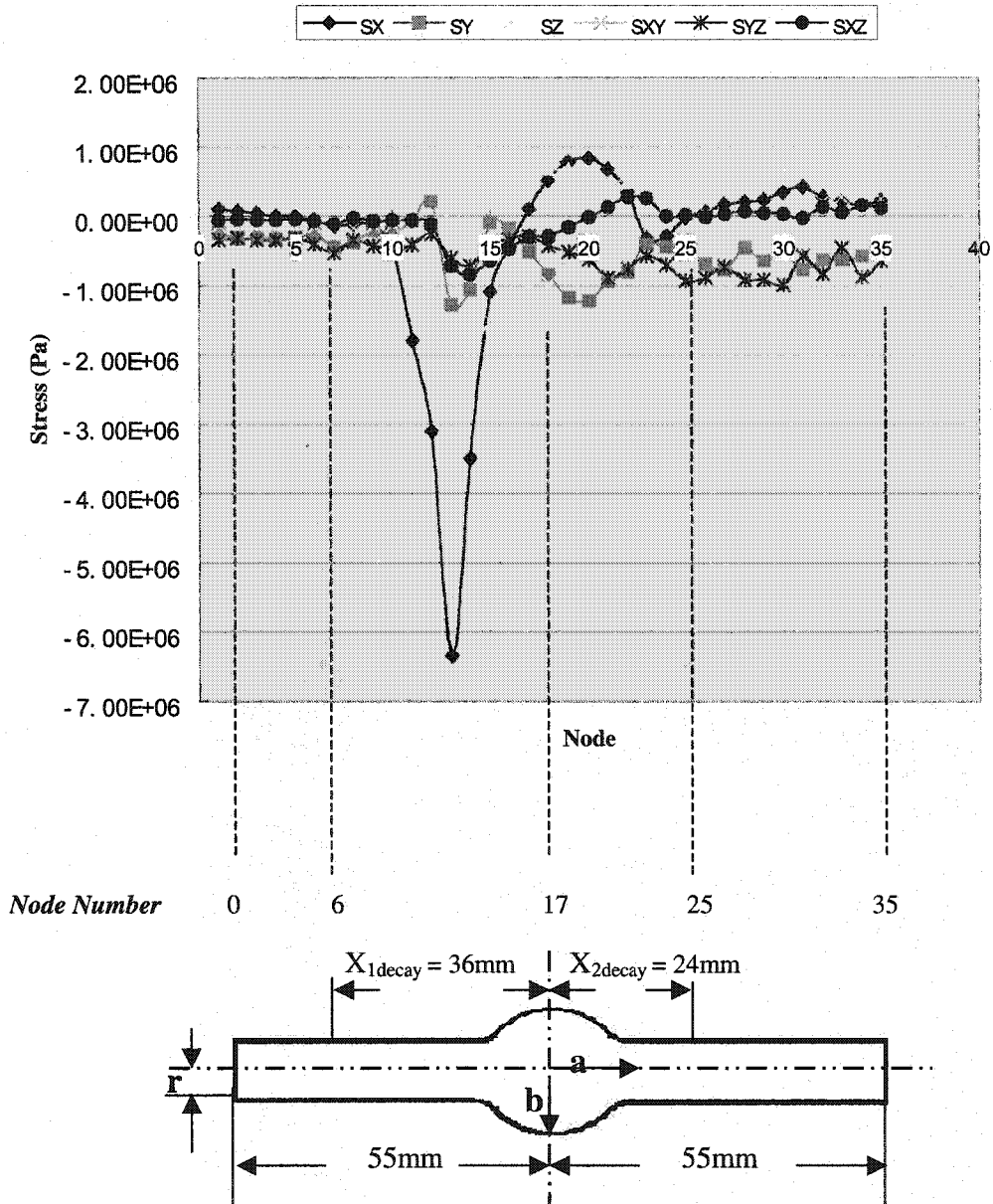
Figure 4.25   **Illustration of distance between two elliptical-shaped**

lobes on FRP rebar

In Figure 4.25 it can be seen that stresses are dieing off from node 17 to node 6 on left

side and from node 17 to node 25 on right side. So if there is another lobe along the

FRP rebar, it can be placed in the area that stresses have died off. The distance for

stress decay can be used as a good estimation for the distance between the lobes.

As illustrated in Figure 4.25,

X_{1decay} = 36mm,

X_{2decay} = 24mm,

Half length of the FRP rebar is 55mm,

Radius of FRP rebar r = 5.5mm,

Major radius of FRP rebar a = 15mm and

Minor radius of FRP rebar b = 11mm,

According to these dimensions distance between the two lobes center L_e should be

$(X_{1decay} * 2)$ mm = 72mm   (For $X_{1decay} > X_{2decay}$).

X_{1decay} -   Distance of stress decay on left side of the lobe

X_{2decay} -   Distance of stress decay on right side of the lobe

L_e -   Distance between two elliptical-shaped lobe centers

So the ratio should be

$r / a / b / L_e$ = 5.5 / 15 / 11 / 72 = 1 / 2.7 / 2 / 13

4.6   Distance guide between two FRP rebars with elliptical-shaped lobes in the concrete

As mentioned in the section 4.3, the distance between the two FRP rebars is an important parameter. For the elliptical-shaped lobe FRP rebars we take the model of FRP rebar with a major radius of 15mm and a minor radius of 11mm elliptical-shaped lobe (Best case in elliptical-shaped lobe models) for consideration. (As shown in Figure 4.26)
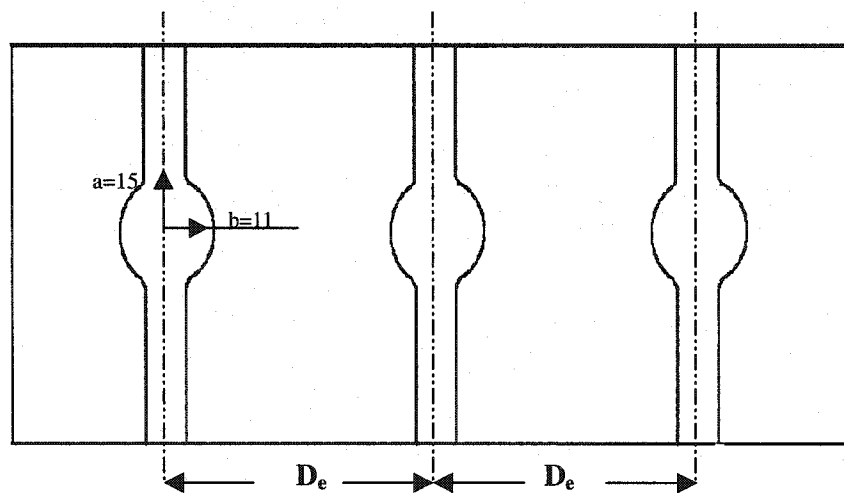
Figure 4.26   Distance between the two FRP rebars

(For elliptical-shaped lobe model)

As studied in the circular-shaped model, one uses the center nodes group UV to give

the distance guide between the two FRP rebars in the concrete system. Figure 4.27

shows the center group nodes chosen from the concrete.
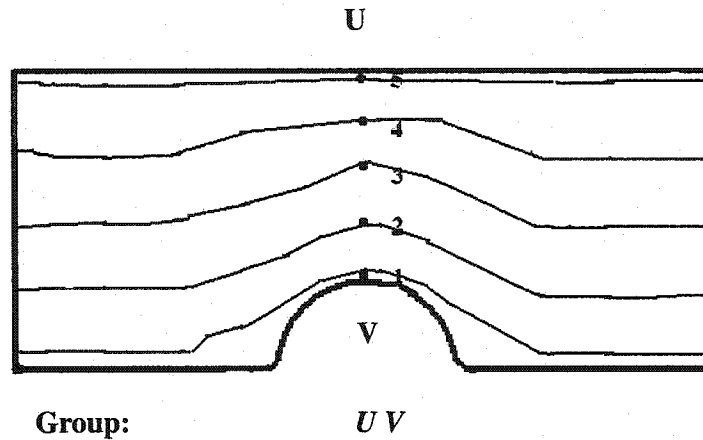
Figure 4.27   **Center nodes group UV for the concrete along the radial**

              direction (Elliptical-shaped lobe model)

Along the center group of nodes, stress distribution along the radial direction in

concrete is shown in Figure 4.28.
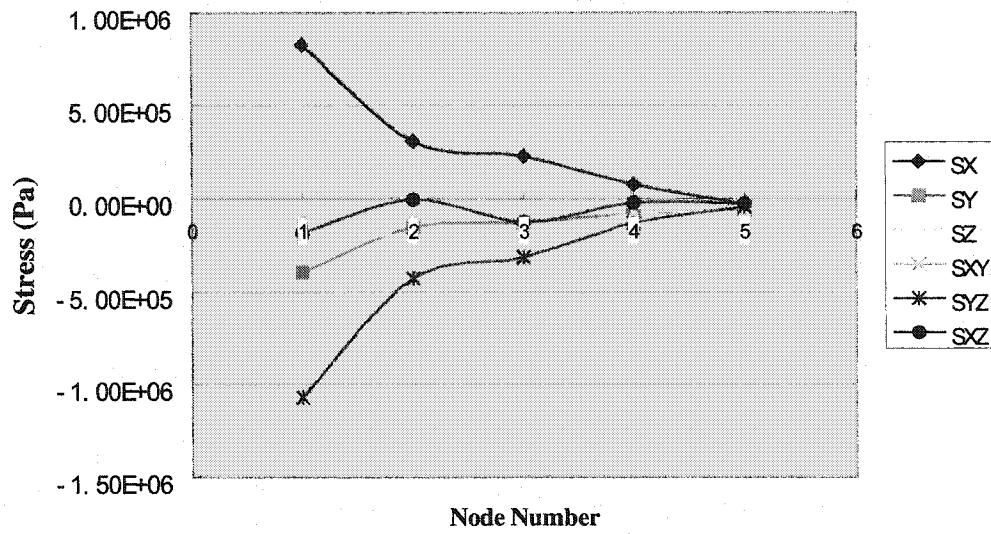
Figure 4.28   **Concrete stress distribution along the radial direction for nodes**

group UV (Elliptical-shaped lobe model)

According to Figure 4.28, it can be seen that from node 3 stresses begin to die off.

Figure 4.29 illustrates how the stress distribution corresponding with the center group

of nodes in the concrete. Dimensions of the model also are shown in this figure.
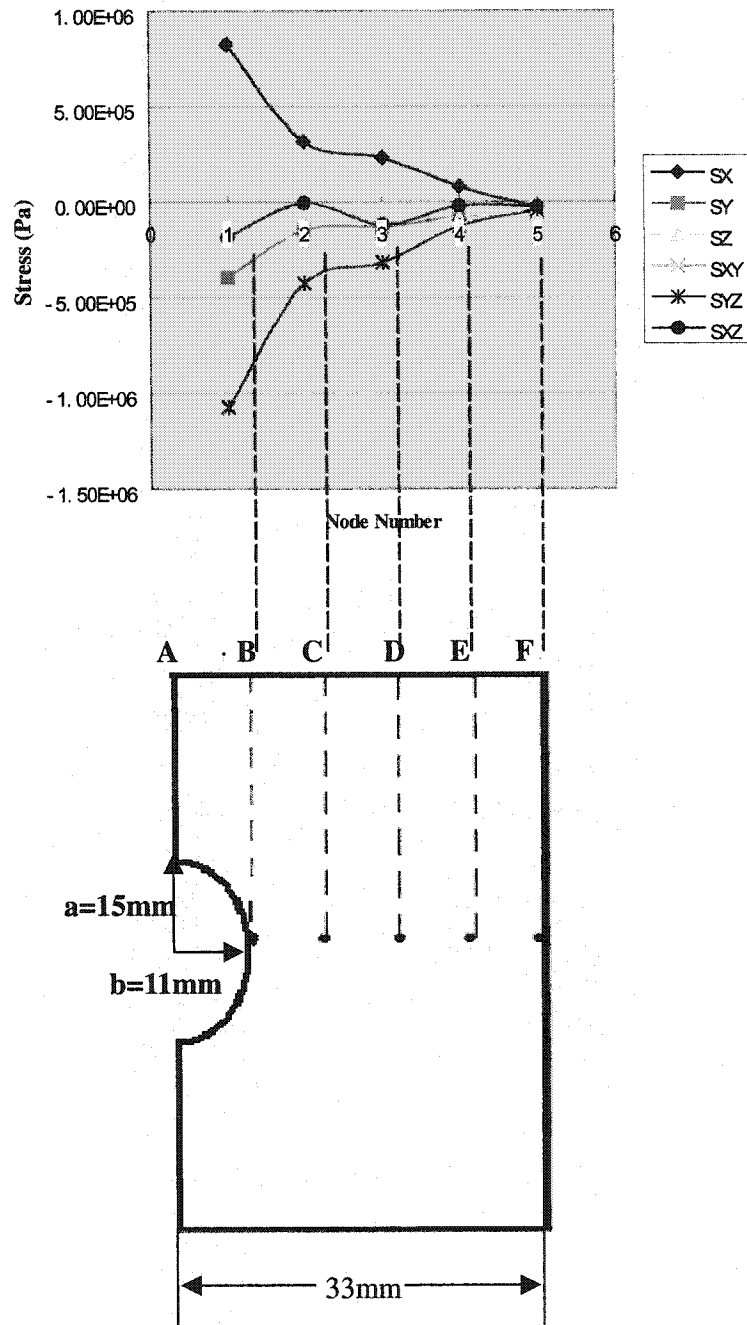
Figure 4.29 Stress distribution corresponding with the nodes group UV in concrete with elliptical-shaped lobe model

According to the dimensions given in Figure 4.29,

Distance between each node is the same BC = CD = DE = EF,

Radius of the concrete is AF = 33mm,

Major radius of the elliptical-shaped lobe is $a = 15$mm,

Minor radius of the elliptical-shaped lobe is $b = 11$mm,

BD = ((33mm − R) / 4)*2 = 11mm,

So the distance between two FRP rebars in the concrete should be

2 * (BD + b) = 44mm

Figure 4.30 shows the configuration between two elliptical-shaped rebars.
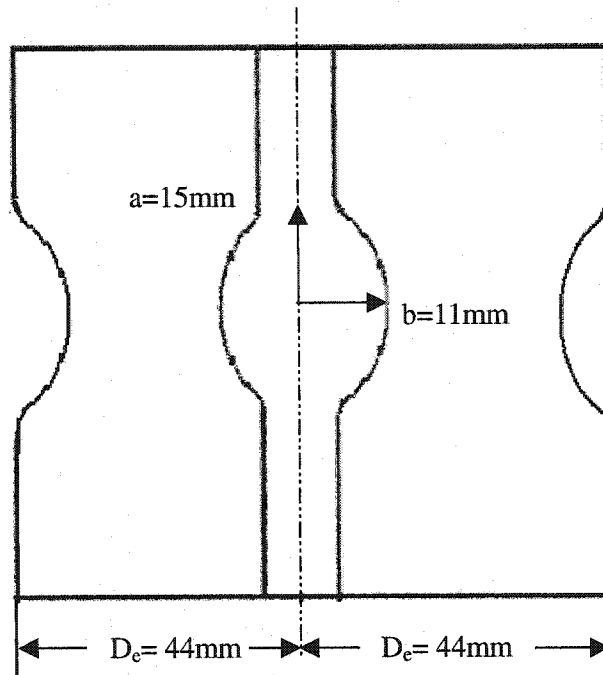
Figure 4.30   **Distance between two or more FRP rebars in the concrete of elliptical-shaped lobe model**

The distance between 2 elliptical-shaped lobes FRP rebar is the same as the model with circular-shaped lobe (44mm). It is because the minor radius b (11mm) of the elliptical-shaped lobe has the same value of the radius (11mm) of the circular-shaped lobe. This means there is no difference in the distance guide as to how far two FRP rebars should be in concrete with elliptical-shaped lobes model and circular-shaped lobes models.

From this it can be concluded that:

For FRP rebar with elliptical-shaped lobe,

Radius of the FRP rebar cross section is r,

Major radius of the elliptical-shaped lobe is a,

Minor radius of the elliptical-shaped lobe is b,

Distance between the two FRP rebars with elliptical-shaped lobes is D_e,

Distance between the two lobes along FRP rebars (With elliptical-shaped lobes) is L_e,

Following is the ratio (As shown in the Figure 4.31):

$$r / a / b / L_e / D_e = 5.5 / 15 / 11 / 72 / 44 = 1 / 2.72 / 2 / 13 / 8$$
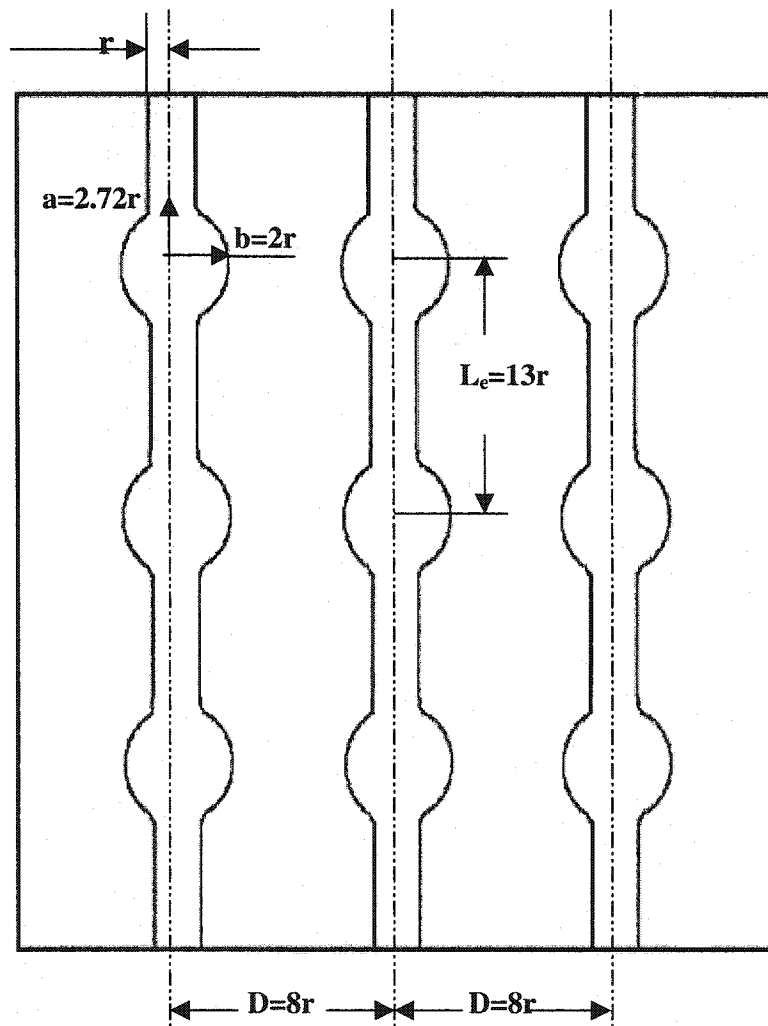
Figure 4.31   Optimal ratio of r, a, b, L_e and D_e

Note that the distance between rebars shown above are for rebars with identical spacing configuration. If one were to mesh the rebars as shown in Figure 4.32, then the distance between the rebars can be less.
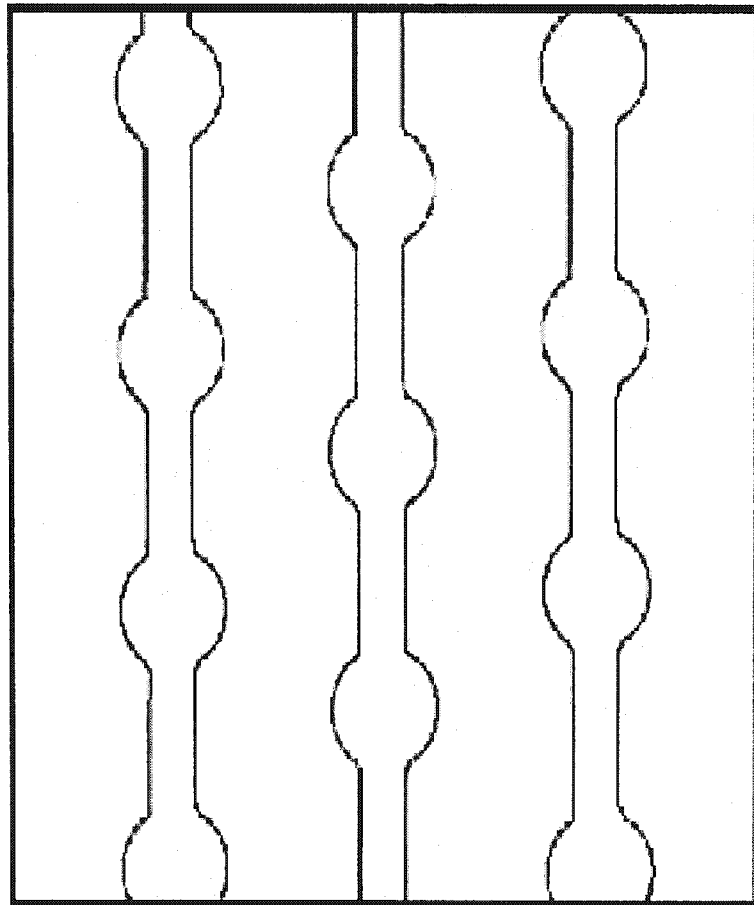
Figure 4.32   Elliptical-shaped rebar with meshed spacing

4.7   Hollow rod versus solid rod. Variation of circular-shaped lobe model. Effect of changing moduli E_2 and E_3

The high cost of composite materials is one of the reasons that prevent them from widespread use. If hollow FRP rebar were used it may be more efficient and the cost can be reduced.

Figure 4.33 shows the optional feature, hole 24 that traverses the length of the reinforcing bar 21 to form a hollow piece. Hole 24 can be provided, for example, to produce a lighter weight reinforcing bar that has a greater circumference to cross-sectional area ratio, which would be advantageous where greater interaction keying of the surface to the concrete is important. A hollow reinforcing bar of this type can be heated and easily crimped in order to bend it or to provide surface irregularities for mechanical interlocking into the concrete. Alternatively, hole 24 can be filled with various materials in order to achieve particular desired product characteristics. For example, hole 24 can be filled with a thermoplastic or thermoset resin, such as off-spec or recycled resin, various fillers such as glass, magnetic, other metallic particles, wood, ceramic or metallic rods [38].
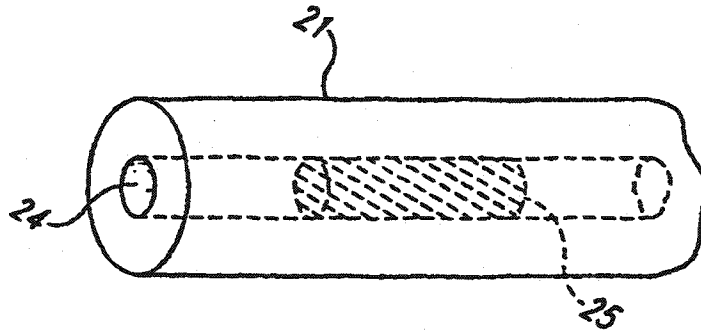
Figure 4.33   **Hollow bar configuration [38]**

As we know, hollow FRP rod is not as stiff in the radial direction as the solid one. In order to investigate the behavior of an FRP rod in concrete using finite element analysis, one can discretize the thickness of the rod in addition to the discretization along the length of the rod and of the concrete. However due to the small thickness of the rod wall the large aspect ratio of the elements for the wall thickness material can give numerical difficulties. Also since the deformation of the rod (Particularly radial deformation) and the stresses in the concrete are important, one may not need to analyze the stresses in the rod in detail. As such, one may consider the case of a solid FRP rod with equivalent stiffness with the hollow rod. Assuming that this equivalent solid rod has the same radius as the outer radius of the hollow rod, the transverse moduli of the solid rod needs to be determined. Due to the lack of an analytical solution for an anisotropic cylinder, an estimation of the moduli of an equivalent rod is determined using the isotropic material solution. This is done as follows:

The case of a rod in concrete subjected to shrinkage of concrete can be considered to be a hollow cylinder subjected to both internal pressure p_i and external pressure p_0 as shown in Figure 4.34. For this the stress and strain are given by [54].

$$\sigma_r = \frac{a_1^2 b_1^2 (p_0 - p_i)}{b_1^2 - a_1^2} \frac{1}{r_1^2} + \frac{p_i a_1^2 - p_0 b_1^2}{b_1^2 - a_1^2} \tag{3}$$

$$\sigma_\theta = -\frac{a_1^2 b_1^2 (p_0 - p_i)}{b_1^2 - a_1^2} \frac{1}{r_1^2} + \frac{p_i a_1^2 - p_0 b_1^2}{b_1^2 - a_1^2} \tag{4}$$

$$\varepsilon_\theta = \frac{1}{E_1}(\sigma_\theta - \nu\sigma_r) \tag{5}$$

Where

a_1 Inner radius of the cylinder

b_1 Outer radius of the cylinder

p_i Uniform internal pressure

p_0 Uniform external pressure

r_1 Radius at any point of cylinder cross-section

σ_r Radial stress

σ_θ Hoop stress

ν Poisson's ratio

ε_θ Hoop strain

E₁   Young's Modulus of hollow isotropic bar
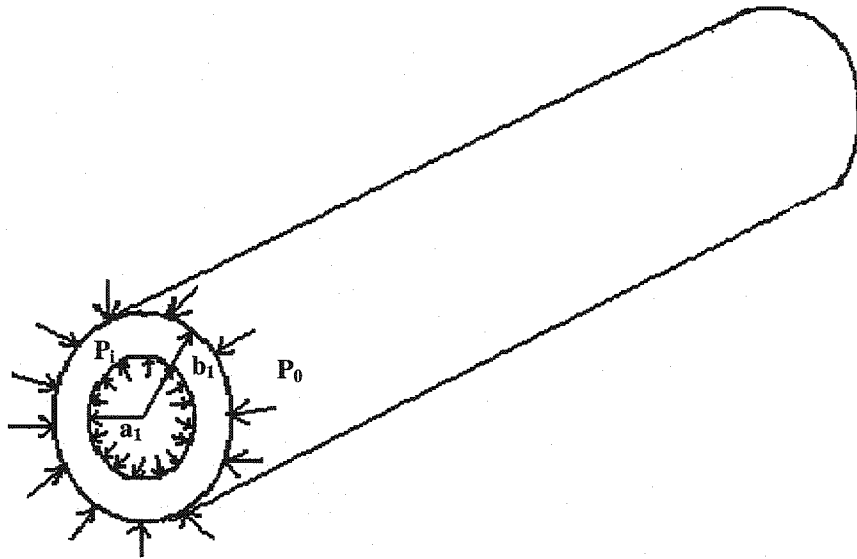
Figure 4.34   Hollow cylinder [54]

Consider also an equivalent solid cylinder with radius b_1 as shown in Figure 4.35. The

strain is given as

$$\varepsilon_\theta = \frac{1}{E_2}(\sigma_\theta - v\sigma_r)$$ (6)

where

E_2 is the Young's Modulus of the solid bar
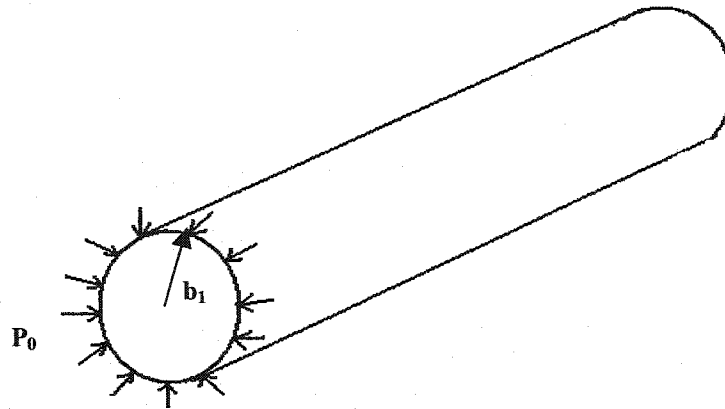
Figure 4.35   Solid FRP rebar case

Assume the hoop strain is the same for the solid FRP rebar and hollow FRP rebar,

equating equations (5) and (6) yield,

$$\frac{1}{E_1}\left(\left(\frac{a_1^2 b_1^2 (p_0 - p_i)}{b_1^2 - a_1^2}\frac{1}{r_1^2} + \frac{p_i a_1^2 - p_0 b_1^2}{b_1^2 - a_1^2}\right) - \nu\left(-\frac{a_1^2 b_1^2 (p_0 - p_i)}{b_1^2 - a_1^2}\frac{1}{r_1^2} + \frac{p_i a_1^2 - p_0 b_1^2}{b_1^2 - a_1^2}\right)\right) =$$

$$\frac{1}{E_2}(p_0 \nu - p_0)$$

At the outer radius, $r_1 = b_1$, substitute in the following values,

$a_1 \quad = b_1 / 2 = 0.00275\text{m}$

$b_1 \quad = 0.0055\text{m}$

$p_i \quad = 0$

$p_0 \quad = p_0$

$$r_1 \quad = b_1 \quad = \quad 0.0055\text{m}$$

yields;

$$\frac{1}{E_2}(p_0 v - p_0) \quad = \quad \frac{1}{E_1}(p_0 v - 1.66 p_0)$$

and with $\quad v = 0.29 \quad$ [55],. We have

$$\frac{E_2}{E_1} \quad = \quad \frac{1}{2}$$

This relation indicates that under same uniform external pressure, if the solid bar and hollow bar were to have the same strain, Young's Modulus of hollow bar E_1 must be twice of the Young's Modulus of solid bar E_2.

So if the solid bar were used to simulate the hollow bar, the radial Modulus of the solid bar should be half that of the hollow rebar.

If one wants to compare the performance of a solid bar and a hollow bar of the same radius b_1, then one can use solid rebar with original moduli E_1, E_2 and E_3 to make model A and one can use E_1, $E_2/2$, $E_3/2$ to make model B to simulate the hollow bar.

Dimensions used in the model are the best case of circular-shaped lobe model (Radius is 11mm circular-shaped lobe). Boundary conditions and force applied are the same as before.

Stress distributions in X, Y, Z, XY, YZ, XZ directions of FRP rebar of circular-shaped

lobe model with original E are shown in Figure 4.36.
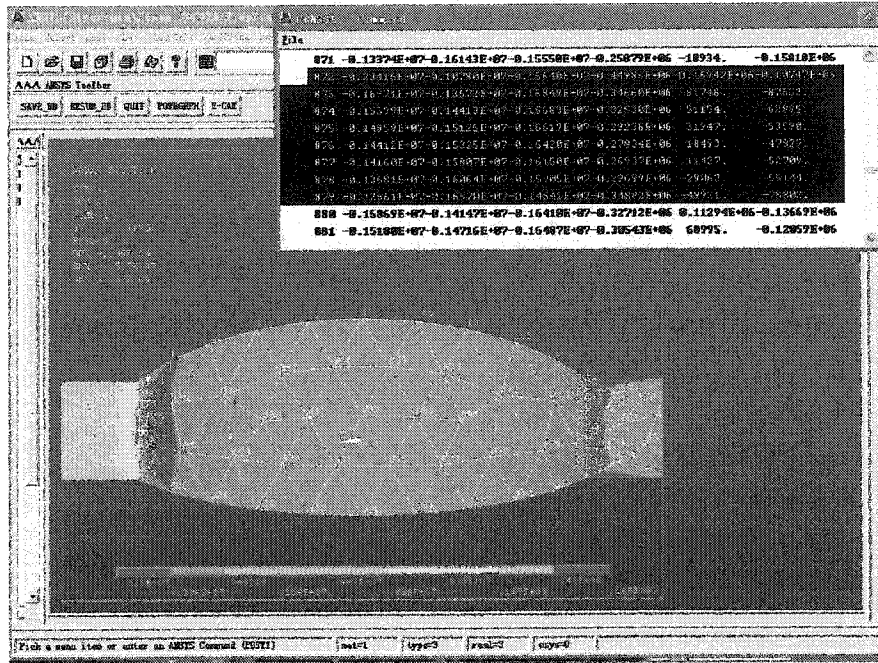
Figure 4.36   Stress distribution of FRP rebar with circular-shaped lobe with

original Young's Moduli E_1, E_2 and E_3

From Figure 4.36, we can choose some nodes on the surface of FRP rebar to obtain

the average Y (Radial), Z directions stresses from the ANSYS® program solution. A

section on the surface of FRP rebar is enlarged and shown in Figure 4.37 and stress

values in Y, Z directions are shown in Table 4.16.
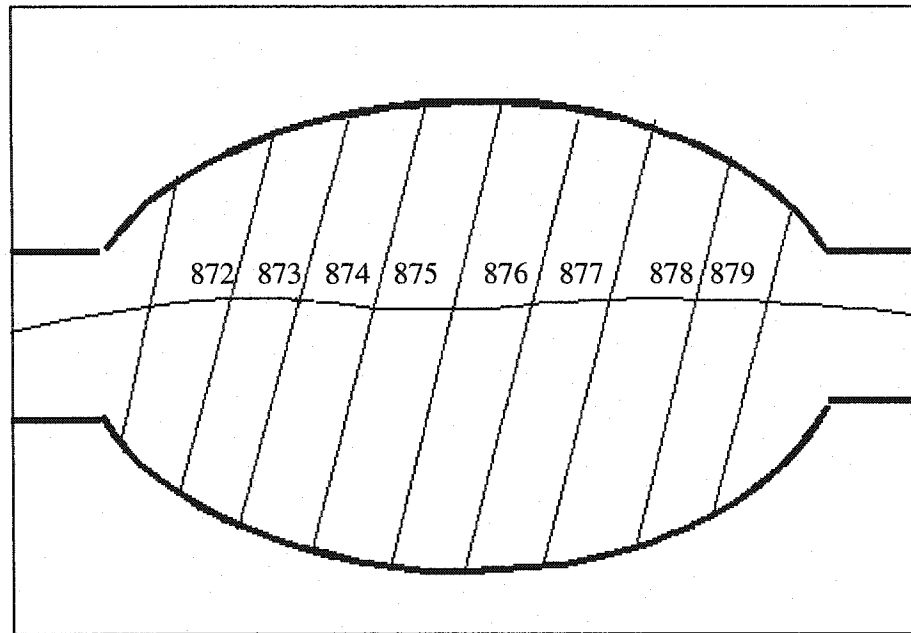
Figure 4.37 Nodes on the surface of FRP rebar with circular-shaped lobe

Table 4.16   Y (Radial), Z directions Stresses of FRP rebar with original Es

(Circular-shaped lobe model)

Nodes number	SY (Pa)	SZ (Pa)
872	-1.078×10^6	-1.664×10^6
873	-1.367×10^6	-1.685×10^6
874	-1.441×10^6	-1.668×10^6
875	-1.513×10^6	-1.662×10^6
876	-1.533×10^6	-1.642×10^6
877	-1.581×10^6	-1.615×10^6
878	-1.606×10^6	-1.591×10^6
879	-1.667×10^6	-1.484×10^6
Average value	$\mathbf{-1.473} \times 10^6$	$\mathbf{-1.624} \times 10^6$

Next, we only change the parameters of E_2, E_3 to 1/2 of the original value. Model B is thus built. Y, Z direction stresses are shown in Table 4.17.

Table 4.17   Y, Z directions Stresses of FRP rebar with half E_2 and half E_3

(Circular-shaped lobe model)

Nodes number	SY (Pa)	SZ (Pa)
872	-0.676×10^6	-0.707×10^6
873	-0.693×10^6	-0.709×10^6
874	-0.703×10^6	-0.713×10^6
875	-0.708×10^6	-0.715×10^6
876	-0.717×10^6	-0.719×10^6
877	-0.723×10^6	-0.718×10^6
878	-0.726×10^6	-0.708×10^6
879	-0.636×10^6	-0.618×10^6
Average value	$\mathbf{-0.698} \times 10^6$	$\mathbf{-0.700} \times 10^6$

Comparing the stresses of FRP rebar of model A and model B Table 4.18 is obtained.

Table 4.18   **Comparison of result of average stresses and radial direction strain**

on FRP rebar when Young's Moduli of FRP rebar are changed

(Circular-shaped lobe model)

Values of FRP rebar Young's Modulus (MPa)	Y direction average stress on FRP rebar (MPa)	Z direction average stress on FRP rebar (MPa)	Radial direction average strain on FRP rebar
$E_1 = 113900$ (Original E) $E_3 = E_2 = 7985$ (Original E)	-1.47	-1.62	-0.36×10^{-4}
$E_1 = 113900$ (Original E) $E_3 = E_2 = 3992.5$ (1/2 original E)	-0.69	-0.70	-1.01×10^{-4}

Young's Modulus is a measure of the stiffness of a material. Small Young's Modulus material results in small stress and large radial direction strains when the same force is applied. Table 4.18 shows the same result as expected.

Following in the same way Table 4.19 is obtained, which shows the average Y, Z directions stress in concrete when changing the Young's Moduli of FRP rebar with circular-shaped lobe.

Table 4.19   Comparison result of average stress in concrete when changing

Young's Moduli of FRP rebar (Circular-shaped lobe model)

Values of FRP rebar Young's Modulus (MPa)	Y direction average stress in concrete (MPa)	Z direction average stress in concrete (MPa)
$E_1 = 113900$ (Original E) $E_3 = E_2 = 7985$ (Original E)	-1.25	-0.68
$E_1 = 113900$ (Original E) $E_3 = E_2 = 3992.5$ (1/2 original E)	-0.63	-0.32

Table 4.19 illustrates that when the Young's Moduli of FRP rebar is reduced the Y,

Z direction average stresses in the reinforced concrete are reduced also.

4.8 Hollow rod versus solid rod. Variation of elliptical-shaped lobe model. Effect of changing moduli E_2 and E_3

For the elliptical-shaped lobe FRP rebar reinforced concrete we use the same method to simulate the hollow FRP rebar. Original parameters of E_1, E_2 and E_3 are used to build the model. Dimensions used are the best case of elliptical-shaped lobe model dimensions (Model #4). Boundary conditions and force applied are the same as used before. From ANSYS® solution, we choose some nodes on the surface of FRP rebar to obtain the average Y, Z direction stress. Comparing the stress and strain of the two FRP rebars, Table 4.20 was obtained.

Table 4.20   Comparison result of average stress and radial direction strain on

FRP rebar when changing Young's Moduli of FRP rebar

(Elliptical-shaped lobe model)

Values of FRP rebar Young's Modulus (MPa)	Y direction average stress on FRP rebar (MPa)	Z direction average stress on FRP rebar (MPa)	Radial direction average strain on FRP rebar
$E_1 = 113900$ (Original E) $E_3 = E_2 = 7985$ (Original E)	-1.45	-1.51	-0.38×10^{-4}
$E_1 = 113900$ (Original E) $E_3 = E_2 = 3992.5$ (1/2 original E)	-0.68	-0.69	-1.00×10^{-4}

Small Young's Modulus material results in small stress and large radial direction strains when the same force applied. Table 4.20 gave the same result as expected.

Table 4.21 shows the average stress in concrete when changing Young's Moduli of

FRP rebar with elliptical-shaped lobe.

Table 4.21   Comparison result of average stress in concrete when changing

Young's Moduli of FRP rebar (Elliptical-shaped lobe model)

Values of FRP rebar Young's Modulus (MPa)	Y direction average stress in concrete (MPa)	Z direction average stress in concrete (MPa)
$E_1 = 113900$ (Original E) $E_3 = E_2 = 7985$ (Original E)	-0.79	-0.43
$E_1 = 113900$ (Original E) $E_3 = E_2 = 3992.5$ (1/2 E)	-0.41	-0.21

According to the analysis above we conclude that the stresses on both FRP rebar and

concrete are reduced when applying the lower Young's Moduli E on the FRP rebar.

The above optimization shows interesting results. The stress in the concrete is lower

for the hollow rebar. It can also reduce the cost of the FRP rebar and reduce the stress

on the reinforcement system at the same time. The only possible drawback would be

larger radial displacement of the rod. (Tables 4.18 and 4.20). This larger radial

deformation may encourage slipping of the rod. However the presence of the lobes

compensates for this.

Chapter 5

Discussion, Conclusion and Suggestion for future work

5.1   Discussion

This new design consists of regular rebar and lobes along the rod that give the bar a wavy configuration. The reinforcement is continuous throughout the rebar and the wavy part contains fibers that are part of the main rebar rather than just bonded in.

The study gives information on optimal design of the geometry of the new rod. Different configurations of the rod give different strengths. Optimal shapes and configurations were discussed. FRP rebar with elliptical-shaped lobes can maximize the efficiency of the reinforcement system.

The replacement of steel with FRP changes the mechanism of load transfer between concrete and reinforcement (FRP). This is because the FRP materials are anisotropic; shear and transverse properties are dominated by the resin and longitudinal properties are dominated by the fiber. No doubt, Fiber Reinforced Plastic rebar reinforced concrete reducs the weight of the system. While the stiffness of the FRP rebar is lower than steel, if in the future higher stiffness FRP rebar can be made with new

manufacturing methods, FRP rebar could be used much widely than now.

The above analysis uses the properties of one type of concrete. However, if the elastic properties (E, υ) of these concretes are the same then the stress should be the same. As long as failure occurs first in concrete the same results (Optimal geometry for rod) should apply.

5.2   Conclusion

Elliptical-shaped rebar

1. Concrete embedded by FRP rebar with elliptical-shaped lobe has less stress than concrete embedded by FRP rebar with circular-shaped lobes when the following relationship was satisfied:

If

Elliptical-shaped lobe major radius is a,

Elliptical-shaped lobe minor radius is b,

FRP rebar cross-section radius is r,

then,

$$R / b = 1 / 2 \quad \text{AND} \quad a / b = 1.36$$

it is the optimized shape.

2. Optimized ratio of distance between two lobes center

If

Elliptical-shaped lobe major radius is a,

Elliptical-shaped lobe minor radius is b,

FRP rebar cross-section radius is r,

and distance between two lobes center is L_e,

the optimized ratio is

$$r / a / b / L_e = 1 / 2.7 / 2 / 13$$

3. Optimized ratio of distance between two FRP rebar

If

Elliptical-shaped lobe major radius is a,

Elliptical-shaped lobe minor radius is b,

and distance between the two FRP rebars with elliptical-shaped lobes is D_e,

the optimized ratio is

$$a / b / D_e \quad = \quad 1.36 / 1 / 8$$

Summarize optimal ratio, relations between the parameters in terms of FRP rebar

(With elliptical-shaped model) radius r are as follows, (Recall Figure 4.31)

$$r \, / \, a \, / \, b \, / \, L_e \, / \, D_e \quad = \quad 1 \, / \, 2.72 \, / \, 2 \, / \, 13 \, / \, 8$$

Figure 4.31 **Optimal ratio of r, a, b, L_e and D_e**

Circular-shaped lobe

1. If it is not possible to produce elliptical-shaped lobes, follow the rule below to
    produce the circular-shaped lobes.

116

If

Circular-shaped lobe radius is R,

FRP rebar cross-section radius is r,

then, the following relationship should be followed.

$$\frac{R}{r} = 2$$
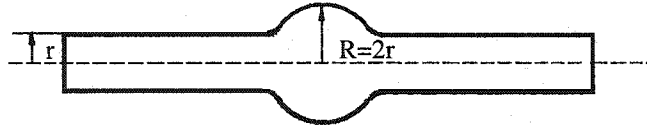
2. Optimized ratio of distance between two lobes center L

If

Circular-shaped lobe radius is R,

FRP rebar cross-section radius is r,

and distance between two lobes center L,

the optimized ratio is

$$r / R / L = 1 / 2 / 9$$

3. Optimized ratio of distance between two FRP rebar

If

Circular-shaped lobe radius is r,

and distance between the two FRP rebars with circular-shaped lobes is D,

the optimized ratio is

$$r/D = 1/8$$

Summarize optimal ratio, relations between the parameters in terms of FRP rebar

(With circular-shaped model) radius r are as follows, (Recall Figure 4.23)

$$r/R/L/D = 1/2/9/8$$

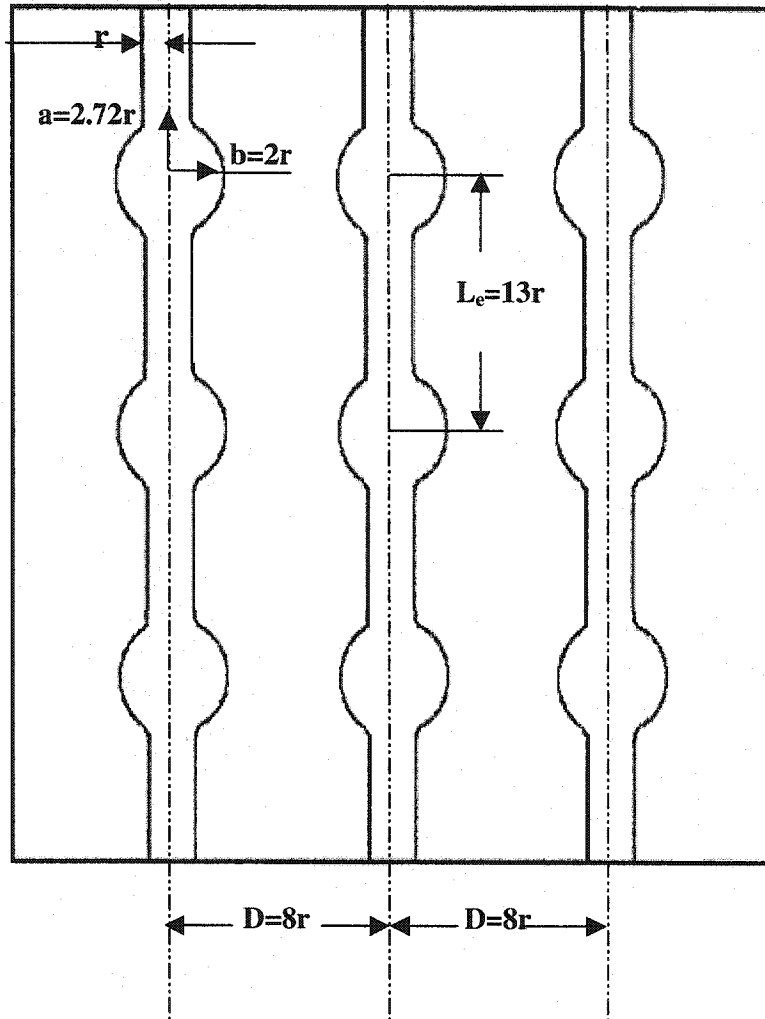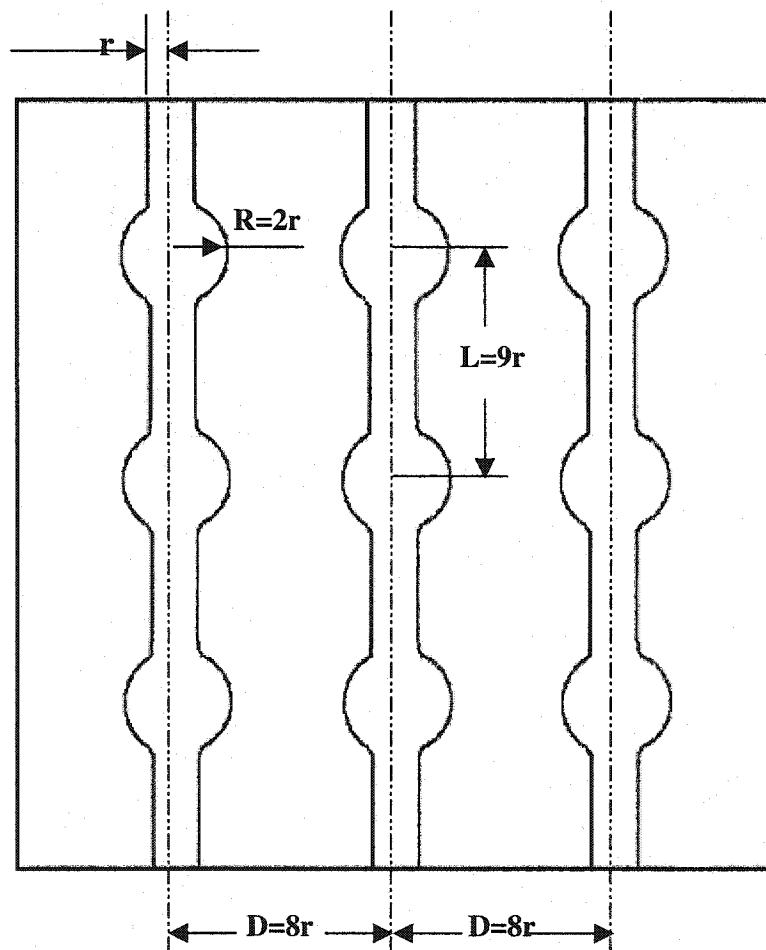**Figure 4.23   Optimal ratio of r, R, L and D**

5.3 Limitation of applicability of the research

The result is valid for the composite and concrete materials use. If other types of concrete or composite material are used, the elastic properties may be different and strength properties can be different. For this case, the optimal dimensions may be different. However, the procedure to obtain the optimal dimension as outlined in the thesis can be used.

The analysis carried out is mainly linear elastic. Even though, contact elements were used. Nonlinear analysis where slipping between the rod and concrete is considered may give more information. The loading conditions considered in the thesis is only axial. In rod life application, there are other models of loading. Such as bending, twisting may exist. Consideration of these models loading may modified the optimal shape of the rod.

5.4 Suggestion for future work

Conclusions mentioned in section 5.2, are calculated by ANSYS®. Experimental works can be done for verifications, like ratios between lobe radius and rod, distance between two lobes along the rod or distance between two rods.

References

1. Muhammad A. "Bond Behavior of Fiber Reinforced Plastic (FRP) Reinforcement with concrete", Ph.D Thesis. The Pennsylvania State University, 1995, pp .1-5.

2. Gowripalan N., Zou, X.W. and Gilbert R.I. "Flexural Behavior of Prestressed Beams Using AFRP Tendons and High Strength Concrete", Advanced composite materials in bridges and structures 2nd international conference, 1996, The Canadian Society for Civil Engineering, pp. 326-327.

3. Saatcioglu M. and Sharbatdar K. "Use of FRP Reinforcement in Concrete Columns", Advanced composite materials in bridges and structures 3rd international conference, 2000, The Canadian Society for Civil Engineering, pp. 363-364.

4. Benmokrane B. and Masmoudi R. "FRP C-Bar as Reinforcing Rod for Concrete Structures", Advanced composite materials in bridges and structures 2nd international conference, 1996, The Canadian Society for Civil Engineering, pp. 182-183.

5. Mallick P. K., "Fiber-Reinforced Composites", 1988, M. Dekker, New York, pp. 1-4, pp. 7-8.

6. Head P. R. "Advanced composites in civil engineering – a critical overview at this high interest, low use stage of development", Advanced composite materials in bridges and structures 2nd international conference, 1996, The Canadian Society for Civil Engineering, pp. 7-8.

7. Rizkalla S.H. "Guide for the Design and Construction of Concrete Reinforced

with FRP Bars", 2000, reported by ACI Committee 440, pp. 14-15.

8. ISIS CANADA, "Reinforcing Concrete Structures with Fibre reinforced Polymers", 2001, Design Manuel. ISIS Canada Corporation, pp. 4.1.

9. Seible F. "Advanced Composites Materials for Bridges in the 21st Century", Advanced composite materials in bridges and structures 2nd international conference, 1996, The Canadian Society for Civil Engineering, pp. 17-18.

10. Erki M.-A., Tadros G. and Machida A. "Avoiding Catastrophic Failure in Concrete Bridges with FRP Reinforcement", Advanced composite materials in bridges and structures 2nd international conference, 1996, The Canadian Society for Civil Engineering, pp. 237-238.

11. Yeung Y.C.T. and Naylor A.W. "Composite Cables for Bridges and Other Structures", Advanced composite materials in bridges and structures 2nd international conference, 1996, The Canadian Society for Civil Engineering, pp. 245-246.

12. Steiner W. "Strengthening of Structures with CFRP Strips", Advanced composite materials in bridges and structures 2nd international conference, 1996, The Canadian Society for Civil Engineering, pp. 407-408.

13. Soudki K.A. and Green M.F. "Performance of CFRP Retrofitted Concrete Columns", Advanced composite materials in bridges and structures 2nd international conference, 1996, The Canadian Society for Civil Engineering, pp. 427-428.

14. Matthys S. and Taerwe L. "Strengthening of Concrete Structures with Externally

Bonded FRP Reinforcement: Some Design Aspects", Advanced composite materials in bridges and structures 3rd international conference, 2000, The Canadian Society for Civil Engineering, pp. 497-498.

15. Taljsten A. "Strengthening of Concrete Structures with CFRP-Sheets: Applications and Full Scale Testes in Sweden", Advanced composite materials in bridges and structures 3rd international conference, 2000, The Canadian Society for Civil Engineering, pp. 513-514.

16. Bisby L.A., Williams B.K., Green M.F. and Kodur V.K.R. "Studies on the Fire Behaviour of FRP Reinforced and /or Strengthened Concrete Members", CDCC Second International Conference, 2002, Sherbrooke University, Canada, pp. 405-406.

17. Saafi M. and Romine P. "Effect of Fire on Concrete Cylinders Confined with FRP", CDCC Second International Conference, 2002, Sherbrooke University, Canada, pp. 511-512.

18. Kato Y., Nishimura T., Uomoto T. and Yamaguchi T. "The Effect of Ultraviolet Rays to FRP Rods", CDCC First International Conference, 1998, Sherbrooke University, Canada, pp. 487-488.

19. Vijay P.V., GangaRao H., Webster K. and Prachasaree W. "Durability of Concrete Beams with Fiber Wraps", CDCC Second International Conference, 2002, Sherbrooke University, Canada, pp. 51-52.

20. Svecova D., Rizkalla S.H., Vogel H. and Jawara A. "Durability of FFRP Bars in Low-Heat High-Performance Concrete", CDCC Second International Conference,

2002, Sherbrooke University, Canada, pp. 75-76.

21. Berman J.B., Trovillion J.C. and Snow C.L. "Natural Weathering Durability Study of Fiber Reinforced Poymer Composites Used as Army Infrastructure Seismic Upgrades", CDCC Second International Conference, 2002, Sherbrooke University, Canada, pp. 63-64.

22. Wang P., Masmoudi R. and Benmokrane B. "Durability of GFRP Bars for Concrete Structures: Assessment and Improvement", CDCC Second International Conference, 2002, Sherbrooke University, Canada, pp. 153-154.

23. Davalos J.F., Qiao P., Trimble B.S. and Jia J. "Durability and Fracture of FRP –Wood Bonded Interfaces", Advanced composite materials in bridges and structures 3rd international conference, 2000, The Canadian Society for Civil Engineering, pp. 695-696.

24. Homam S.M., Sheikh S.A., Collins P., Pernica G. and Daoud J. "Durability of Fiber Reinforced Polymers Used in Concrete Structures", Advanced composite materials in bridges and structures 3rd international conference, 2000, The Canadian Society for Civil Engineering, pp. 751-752.

25. Pando M., Lesko J., Fam A. and Rizkalla S. "Moisture Effect on Durability of Axially Loaded Concrete-Filled Tubular FRP Piles", CDCC Second International Conference, 2002, Sherbrooke University, Canada, pp. 25-26.

26. Phifer S.P. and Lesko J. "Moisture Absorption and Strength Characterization of Hygrothermally Aged Neat and Clay Filled Vinylester and Pultruded Vinylester E-Glass Laminates", CDCC Second International Conference, 2002, Sherbrooke

University, Canada, pp. 485-486.

27. Ferrier E. and Hamelin P. "Effect of Water Absorption on the Durability of Carbon FRP Reinforcement", CDCC Second International Conference, 2002, Sherbrooke University, Canada, pp. 99-100.

28. Shao Y. and Kouadio S. "Water Absorption of FRP Seawall Panels", CDCC Second International Conference, 2002, Sherbrooke University, Canada, pp. 587-588.

29. Uomoto T. and Ohga H. "Performance of Fiber Reinforced Plastics for Concrete Reinforcement", Advanced composite materials in bridges and structures 2nd international conference, 1996, The Canadian Society for Civil Engineering, pp. 125-126.

30. Al-Dulaijan S.U., Nanni A., Al-Zahrani M.M., Bakis C.E., Boothby T.E. "Bond Evaluation of Environmentally Conditioned GFRP/Concrete Systems", Advanced composite materials in bridges and structures 2nd international conference, 1996, The Canadian Society for Civil Engineering, pp. 845-846.

31. Al-Dulaijan S.U., Nanni A., Al-Zahrani M.M., Bakis C.E. "Bond of FRP to Concrete in Reinforcement Rods with Axisymmetric Deformations", Advanced composite materials in bridges and structures 2nd international conference, 1996, The Canadian Society for Civil Engineering, pp. 853-854.

32. Faoro M. "The Influence of Stiffness and Bond of FRP Bars and Tendons on the Structural Behaviour of Reinforced Concrete Members", Advanced composite materials in bridges and structures 2nd international conference, 1996, The

Canadian Society for Civil Engineering, pp. 885-886.

33. Benmokrane B., Tighiouart B. and O. Chaallal, "Bond strength and load distribution of composite GFRP reinforcing bars in concrete", 1996, ACI Materials Journal, May-June, pp. 246-253.

34. Nanni A., Al-Zaharani M.M., Al-Dulaijan S.U., Bakis C.E. and Boothby T.E. "Bond of FRP reinforcement to concrete-experimental results", Proc.2nd Inter. RILEM Symposium, L. Taerwe, ed. E&FN Spon. London, 1995, pp. 135-145.

35. Cosenza E., Manfredi G. and Realfonzo R. "Behavior and modeling of bond of FRP rebars to concrete', J.Composite for Construction, ASCE, 1997, Vol.2, No.2, pp. 40-51.

36. Nobuyuki O., Junji H, Masao K., Tokitaro H. and Kinsuke Y. "European Patent Application", 1993, Publication Number: 0560362A2, pp. 3-19.

37. Edwards C. M. and D'Hooghe E.L. "United States Patent Application Publication", 2001, Publication Number: US 2001/0023568 A1, pp. 1- 4.

38. Arumugasaamy P. and Greenwood M.E. "Tnited States Patent", 1998, Patent Number: 5,727,357, pp. 1-12.

39. Hoa, S.V. "A new composite rod for the reinforcement of concrete", 2003, Patten pending.

40. Akroyd T.N.W. "Concrete properties and manufacture", 1962, Pergamon press, pp. 1–25.

41. Baker T, "Making and placing concrete", 1985, Longman group (FE) Ltd, pp. 1–11.